
BAYESIAN COPULA-BASED MODELLING FOR MULTI-TYPE SPATIO-TEMPORAL EPIDEMIC DATA

Matthew Adeoye
Department of Statistics
University of Warwick

Simon E.F. Spencer
Department of Statistics
University of Warwick

Xavier Didelot
School of Life Sciences and
Department of Statistics
University of Warwick

May 6, 2026

ABSTRACT

The study of infectious disease epidemiology for multi-type disease pathogens requires modelling techniques that account for the complex interactions existing between strains across geography and time. In this paper, we propose a novel multi-type spatio-temporal infectious disease model to better support the understanding of these pathogens. We formulate a joint state-space for all epidemics arising for a given multi-type pathogen as well as biologically informed representations of how these epidemic states may interact. We introduce the use of several copula models to uncover the dependence structure of epidemics between strains. We develop a computationally efficient Markov chain Monte Carlo (MCMC) sampling scheme for all proposed models. We also provide robust model comparison techniques using bridge sampling and importance sampling to evaluate model evidence in high-dimensional space. We demonstrate the performance of our proposed models using simulated datasets, where simulated epidemics were successfully identified and associated parameters correctly inferred. The proposed models were also fitted to monthly multi-type incidence data on invasive meningococcal disease from 26 European countries. The accompanying software is freely available as a R package at <https://github.com/Matthewadeoye/MultiOutbreaks>.

1 Introduction

Infectious disease surveillance often includes typing of at least a subset of the reported infected cases. One of the oldest and most popular typing method is serotyping, in which antibodies are used to detect the presence of antigens on the surface of the pathogen. Over a century after it was first proposed [1], serotyping is still in widespread use for both bacterial pathogens such as *Streptococcus pneumoniae* [2] or *Neisseria meningitidis* [3] and viral pathogens such as influenza [4] or foot-and-mouth disease [5]. There are many other typing methods depending on the disease, with the most recent ones being based on molecular sequences, such as multi-locus sequence typing (MLST) for bacteria [6], real-time polymerase chain reaction (PCR) for DNA viruses [7] and real-time reverse transcription PCR for RNA viruses [8]. In the remainder of this paper we consider that an infectious disease can be subdivided into several types, irrespective of the exact typing method being used.

The most commonly used mathematical models of infectious disease epidemiology take a compartmental form [9]. For example, the famous SIR model divides individuals in the population into three compartments: susceptible, infected and removed [10]. Compartmental models can be extended in many ways, including to handle typing data, by duplicating the compartments corresponding to infected individuals as many times as there are types [11]. Additional parameters can then be used in the rates of transition between compartments to represent the many types of interactions that may exist between types. In particular, infection with one type may result in immunity, at least for some time, to re-infection with the same type, but may also result in cross-immunity, that is partial or complete immunity to subsequent infection with other types [12, 13, 14]. The possibility of superinfection with more than one type simultaneously may also be important to take into account for some diseases, resulting in additional compartments with specific dynamic properties [15, 16].

Here we focus on a different class of infectious disease model, specifically designed to analyse spatio-temporal data, where a number of cases is observed for each spatial and temporal unit [17, 18, 19]. In this context, the joint modelling of multiple types has not yet been explored as for compartmental models. Consequently, analysis of multi-type data with currently existing spatio-temporal methods requires to either analyse each type separately, or aggregate all types as a single disease. Neither of these two approaches can reveal interactions between types, even though this is often the most important aspect to understand the mechanisms of disease spread and how epidemics arise. For example, cross-immunity has a long history of being studied using compartmental models [12, 13, 14] but can not currently be studied using spatio-temporal models. Interaction between types is also crucial to take into account when formulating control intervention strategies for many infectious diseases, including influenza [20, 21], antibiotic resistant gonorrhoea [22, 23] and COVID-19 [24, 25].

We take as a starting point a previously proposed framework for Bayesian spatio-temporal modelling for infectious disease epidemiology analysis [17, 26, 27] and restructure it to enable the joint analysis of multiple types. We propose to model the joint dynamics of multiple disease types using copulas [28], which has the desirable property of separating their interdependency from their marginal behaviour. The resulting models are complex with many parameters, but we show that Bayesian inference can still be performed at scale using a carefully designed Metropolis adjusted Langevin algorithm [29]. We evaluate the usefulness of this new inferential methodology using simulated datasets, in which the correct model and parameter values are known so that the accuracy of inferred values can be assessed. We also showcase the practical use of our methodology with an application to real data on the incidence of the main four serogroups of invasive meningococcal disease across European countries [30].

2 Methods

2.1 Model structure

Let y_{it} and e_{it} denote the number of cases and the size of the population at risk at location i at time t , respectively for $i = 1, \dots, I$ and $t = 1, \dots, T$. The observed case counts, y_{it} , conditional on the risks λ_{it} , are assumed to follow a Poisson distribution:

$$y_{it} | \lambda_{it} \sim \text{Poisson}(e_{it} \lambda_{it}). \quad (1)$$

We decompose the logarithmic risk of disease incidence into a temporal trend component (r_t), a seasonal component ($s_{t \bmod C}$), a spatial component (u_i), a spatio-temporal epidemic indicator ($x_{it} = 1$ for the epidemic state and $x_{it} = 0$ for the endemic state), and an increased risk factor during epidemics (β):

$$\log(\lambda_{it}) = a + r_t + s_{t \bmod C} + u_i + x_{it} \beta. \quad (2)$$

The epidemic indicator x_{it} is ruled by a time-homogeneous Markov chain. Note that this model corresponds to the model VII proposed by [27].

2.2 Multi-type disease pathogens

Let us consider that there are $K \in \mathbb{N}$ strains of the disease pathogen being studied, and we are interested in epidemics in all strains, both marginally and jointly. We extend the model in Equation 1 as follows:

$$y_{itk} | \lambda_{itk} \sim \text{Poisson}(e_{it} \lambda_{itk}). \quad (3)$$

The simplest formulation of the logarithmic risk λ_{itk} in Equation 3 is to assume that there are K independent epidemic terms for all K types of disease pathogens observed:

$$\log(\lambda_{itk}) = a_k + r_t + s_{t \bmod C} + u_i + x_{itk} \beta_k. \quad (4)$$

The difference with the previous model in Equation 2 is that a_k is the intercept for the k -th pathogen and β_k is the increased risk factor associated with the k -th epidemic term (x_{itk}). A graphical illustration of the model is shown in Figure 1.

2.2.1 Spatio-temporal model for the sporadic cases

The spatio-temporal model for the sporadic cases excludes the epidemic component in Equation 4, where a_k remains the strain-specific intercept. The trend, seasonal and spatial components are given priors from the family of intrinsic Gaussian Markov random fields [31], designed to induce smoothness in either space or time. The trend component r_t is assumed to follow a smooth second-order random walk model given by:

$$r_t | r_{t-1}, r_{t-2} = 2r_{t-1} - r_{t-2} + \epsilon_t, \quad (5)$$

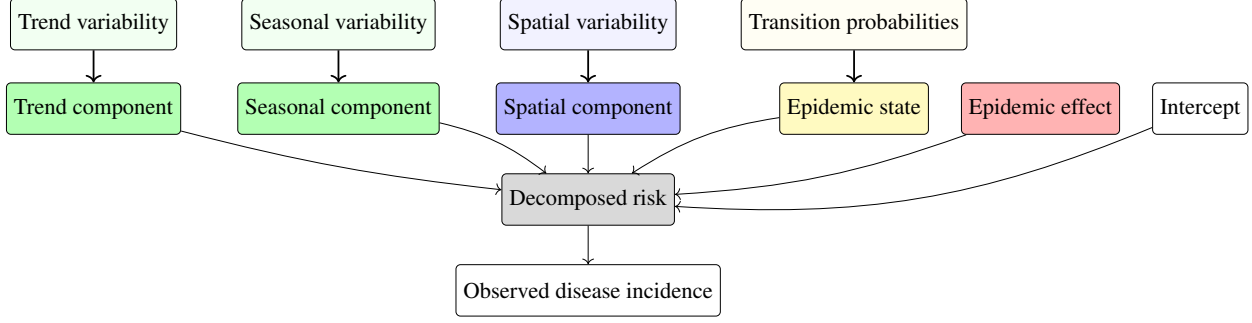


Figure 1: Directed acyclic graph (DAG) illustrating the relationships between all model components and the observed disease incidence.

where $\epsilon_t \sim \mathcal{N}(0, \kappa_r^{-1})$ and κ_r is the precision parameter. Similarly, the seasonal component $s_{t \bmod C}$ is assumed to follow a cyclical first-order random walk written as:

$$s_c = s_{c-1} + \epsilon_c, \quad (6)$$

where $\epsilon_c \sim \mathcal{N}(0, \kappa_s^{-1})$, κ_s is the precision parameter, $c = 2, \dots, C$, and then $s_1 - s_C \sim \mathcal{N}(0, \kappa_s^{-1})$ so that s_1 and s_C are considered neighbouring components. Lastly, the spatial component u_i is assumed to follow an intrinsic conditional autoregression (ICAR) model which acts as a spatial smoothing prior and is typically written as:

$$u_i = \frac{1}{|n(i)|} \sum_{j \in n(i)} u_j + \epsilon_i, \quad (7)$$

where $n(i)$ is the set of indices of locations that neighbour location $i \in \{1, \dots, I\}$, and $\epsilon_i \sim \mathcal{N}(0, \frac{1}{|n(i)|\kappa_u})$, κ_u is the precision parameter. These temporal and spatial components are assumed to be constant across all strains. Full details on these prior distributions are provided in Appendix Sections A.1, A.2, and A.3.

2.2.2 Joint state-space formulation for the epidemic cases

Let us now consider the joint state-space for epidemics in all K strains. We define $\mathbf{x}_{it} = (x_{it1}, x_{it2}, \dots, x_{itK}) \in \{0, 1\}^K$ to be a Markov process over time t with transition matrix Γ . A first model is to consider that epidemics of the different strains happen independently and according to the same Markov chain with 2x2 transition matrix γ . For example, if there are $K = 2$ strains each ruled by $\gamma = \begin{pmatrix} 1-p & p \\ q & 1-q \end{pmatrix}$ then the resulting joint transition probability matrix is:

$$\Gamma = \begin{matrix} & \begin{matrix} (0,0) & (0,1) & (1,0) & (1,1) \end{matrix} \\ \begin{matrix} (0,0) \\ (0,1) \\ (1,0) \\ (1,1) \end{matrix} & \begin{pmatrix} (1-p)^2 & (1-p)p & p(1-p) & p^2 \\ (1-p)q & (1-p)(1-q) & pq & p(1-q) \\ q(1-p) & qp & (1-q)(1-p) & (1-q)p \\ q^2 & q(1-q) & (1-q)q & (1-q)^2 \end{pmatrix} \end{matrix} \quad (8)$$

To write down the general case $K \geq 2$ we need to consider how the i -th state of the joint model relates to the epidemic state for each of the K strains. We use the following encoding: the state $i \in \{0, \dots, 2^K - 1\}$ is such that there is an epidemic of the k -th strain if the k -th bit of i is one. Extracting the k -th bit of i is done via integer division and modulo:

$$\text{bit}(i, k) = \left\lfloor \frac{i}{2^{k-1}} \right\rfloor \bmod 2$$

We can then write down the transition probability from state i to state j as:

$$\Gamma_{i,j} = \prod_{k=1}^K \gamma_{\text{bit}(i,k), \text{bit}(j,k)} \quad \text{for } i, j \in \{0, \dots, 2^K - 1\}. \quad (9)$$

An alternative model is to consider that epidemics of the different strains happen independently, but each is ruled by its own unique transition probability matrix, $\gamma^{(k)}$. In this case the joint transition matrix is:

$$\Gamma_{i,j} = \prod_{k=1}^K \gamma_{\text{bit}(i,k), \text{bit}(j,k)}^{(k)} \quad \text{for } i, j \in \{0, \dots, 2^K - 1\}. \quad (10)$$

2.2.3 Copulas

Sklar's theorem states that any multivariate cumulative distribution function (CDF), $F(\mathbf{x}) = \mathbb{P}(X_1 \leq x_1, \dots, X_K \leq x_K)$ can be expressed in terms of its univariate marginal distributions $F_i(x_i) = \mathbb{P}(X_i \leq x_i)$ and a copula function $C : [0, 1]^K \rightarrow [0, 1]$ such that $F(\mathbf{x}) = C(F_1(x_1), \dots, F_K(x_K))$ [32]. A copula therefore captures the dependence structure of a vector of random variables, separately from their marginal behaviours. There are many copula families in the literature [33, 34, 28], each modelling specific dependence structures that allow flexible representation of complex multivariate relationships. In this paper, we consider the Frank copula and the Gaussian factor copula model.

A K -dimensional Frank copula, for any $\mathbf{u} \in [0, 1]^K$, is defined as:

$$C_\psi(\mathbf{u}) = -\psi^{-1} \log \left\{ 1 - \frac{\prod_{k=1}^K (1 - \exp(-\psi u_k))}{(1 - \exp(-\psi))^{K-1}} \right\}. \quad (11)$$

The Frank copula has a single parameter with support $\psi \in \mathbb{R} \setminus \{0\}$ for the bivariate case, and $\psi \in \mathbb{R}^+$ for any dimension $K \geq 3$, and this parameter characterizes the dependence structure between the variables. The multivariate Frank copula with dimension $K \geq 3$ can only model positive dependence structure due to its inability to satisfy the monotonicity constraint on its generator for negative dependence structures [33]. In contrast, the bivariate Frank copula satisfies the monotonicity constraint for both positive and negative dependence structures and has the following interpretation: (i) $\psi \rightarrow 0$ corresponds to independence, (ii) $\psi > 0$ corresponds to a positive dependence structure, and (iii) $\psi < 0$ corresponds to a negative dependence structure.

A K -dimensional Gaussian copula is the copula obtained via Sklar's theorem from the multivariate Gaussian distribution $\mathcal{N}_K(\mathbf{0}, \Sigma)$ with correlation matrix Σ . Note that Σ is both the correlation and covariance matrix here since the random variables (x_1, \dots, x_K) are standard normal variates. If Φ_Σ denotes the multivariate Gaussian cumulative distribution function, the copula C_Σ is given, for any $\mathbf{u} \in [0, 1]^K$ by

$$\begin{aligned} C_\Sigma(\mathbf{u}) &= \Phi_\Sigma(\Phi^{-1}(u_1), \dots, \Phi^{-1}(u_K)) \\ &= \int_{-\infty}^{\Phi^{-1}(u_K)} \dots \int_{-\infty}^{\Phi^{-1}(u_1)} \frac{\exp(-\frac{1}{2} \mathbf{x}^\top \Sigma^{-1} \mathbf{x})}{(2\pi)^{K/2} \sqrt{\det \Sigma}} dx_1 \dots dx_K, \end{aligned} \quad (12)$$

where Φ^{-1} denotes the quantile function of $\mathcal{N}(0, 1)$. However, the K -dimensional Gaussian copula typically requires evaluating a K -dimensional integral, which is computationally intensive as K increases. We consider the factor copula model proposed to capture tail dependence and asymmetries in multivariate data while offering parsimony and significant computational advantages over the multivariate Gaussian copula [35]. The Gaussian factor copula model attempts to explain the dependence structure in the observed variables by one or more latent variables. For example, the j -factor copula assumes $\mathbf{u} = (u_1, \dots, u_K)$ to be conditionally independent given j latent variables V_1, \dots, V_j , where the latent variables are assumed to be independently and identically distributed as $\text{Uniform}(0, 1)$. Let the conditional CDF and copula of the k th variable given V_1, \dots, V_j be denoted as $F_{k|V_1, \dots, V_j}$ and $C_{k|V_1, \dots, V_j}$ respectively. Then

$$C(\mathbf{u}) = \int_0^1 \dots \int_0^1 \prod_{k=1}^K F_{k|V_1, \dots, V_j}(u_k | v_1, \dots, v_j) dv_1 \dots dv_j.$$

Similarly, the 1-factor copula model conditions each marginal distribution on a common latent variable V_1 and is written as:

$$C(u_1, \dots, u_K) = \int_0^1 \prod_{k=1}^K F_{k|V_1}(u_k | v_1) dv_1 = \int_0^1 \prod_{k=1}^K C_{k|V_1}(u_k | v_1) dv_1.$$

Suppose $u_k = \Phi(x_k)$, then the 1-factor copula model using a bivariate Gaussian copula with correlation parameter ξ_{k1} for linking the k -th strain with the latent variable V_1 , is written as:

$$C(\Phi(x_1), \dots, \Phi(x_K)) = \int_0^1 \prod_{k=1}^K \Phi \left(\frac{x_k - \xi_{k1} \Phi^{-1}(v_1)}{\sqrt{1 - \xi_{k1}^2}} \right) dv_1 = \int_{-\infty}^{\infty} \left\{ \prod_{k=1}^K \Phi \left(\frac{x_k - \xi_{k1} w}{\sqrt{1 - \xi_{k1}^2}} \right) \right\} \phi(w) dw, \quad (13)$$

where Φ and ϕ represent the Gaussian cumulative distribution function and probability density function, respectively. The correlation parameters $\{\xi_{k1} : k = 1, \dots, K\}$ between each disease strain and the latent variable are referred to as factor loadings. Thus, the dependence structures between the variables (x_1, \dots, x_K) are derived from factor loadings, such as $\text{Corr}(x_k, x_l) = \xi_{k1} \times \xi_{l1}$.

2.2.4 Epidemic dependence modelling via copulas

Through the use of copulas, we can relax the assumption of independence in transitions between strains. Let us once again consider first the case $K = 2$. Let $C(u, v)$ denote an arbitrary bivariate copula where u and v denote the marginal probabilities that strains 1 and 2 transit to the epidemic state 1 in the next step, respectively. The four joint probabilities follow from Sklar's theorem and the inclusion-exclusion principle [28, 34]:

$$\begin{aligned}\mathbb{P}(X_t = (0, 0)|X_{t-1}) &= 1 - u - v + C(u, v), \\ \mathbb{P}(X_t = (0, 1)|X_{t-1}) &= v - C(u, v), \\ \mathbb{P}(X_t = (1, 0)|X_{t-1}) &= u - C(u, v), \\ \mathbb{P}(X_t = (1, 1)|X_{t-1}) &= C(u, v).\end{aligned}$$

Assuming the two strains have the same transition matrix $\gamma = \begin{pmatrix} 1-p & p \\ q & 1-q \end{pmatrix}$, then the elements of the joint transition matrix are obtained by replacing (u, v) with (p, p) for the transitions from state $(0, 0)$; with $(p, 1-q)$ for the transitions from state $(0, 1)$; with $(1-q, p)$ for the transitions from state $(1, 0)$; and with $(1-q, 1-q)$ for the transitions from state $(1, 1)$. These calculations are detailed in the Appendix A.4, as well as for the case $K = 3$ in Appendix A.5. Gathering these terms into a matrix gives the transition matrix:

$$\mathbf{\Gamma} = \begin{matrix} & \begin{matrix} (0, 0) & (0, 1) & (1, 0) & (1, 1) \end{matrix} \\ \begin{matrix} (0, 0) \\ (0, 1) \\ (1, 0) \\ (1, 1) \end{matrix} & \begin{pmatrix} 1-2p+C(p, p) & p-C(p, p) & p-C(p, p) & C(p, p) \\ q-p+C(p, 1-q) & 1-q-C(p, 1-q) & p-C(p, 1-q) & C(p, 1-q) \\ q-p+C(1-q, p) & p-C(1-q, p) & 1-q-C(1-q, p) & C(1-q, p) \\ 2q-1+C(1-q, 1-q) & 1-q-C(1-q, 1-q) & 1-q-C(1-q, 1-q) & C(1-q, 1-q) \end{pmatrix} \end{matrix}. \quad (14)$$

Note that the transition matrix for the independent model (Equation 8) is a special case of the dependent model (Equation 14) if we use the independence Copula $C(u, v) = uv$. Generalization to the case $K \geq 2$ follows directly from the inclusion-exclusion principle and requires a K -dimensional multivariate copula, C . Let $\mathcal{S} = \{k : \text{bit}(j, k) = 1\}$ be the set of strains for which there are epidemics in state j , and let $\mathcal{S}^c = \{k : \text{bit}(j, k) = 0\}$ be its complement.

If all strains have the same transition probability matrix γ then each element of the copula-dependent joint transition probability matrix is given by:

$$\Gamma_{i,j} = \sum_{\mathcal{T} \subseteq \mathcal{S}^c} (-1)^{|\mathcal{T}|} C \left(\left\{ (\gamma_{\text{bit}(i,k),1})^{\mathbb{1}_{(k \in \mathcal{S} \cup \mathcal{T})}} : k = 1, \dots, K \right\} \right). \quad (15)$$

If on the other hand each strain has its own transition probability matrix $\gamma^{(k)}$ then:

$$\Gamma_{i,j} = \sum_{\mathcal{T} \subseteq \mathcal{S}^c} (-1)^{|\mathcal{T}|} C \left(\left\{ (\gamma_{\text{bit}(i,k),1}^{(k)})^{\mathbb{1}_{(k \in \mathcal{S} \cup \mathcal{T})}} : k = 1, \dots, K \right\} \right). \quad (16)$$

Finally, we can define the general-dependent model to be any Markov matrix $\mathbf{\Gamma}$ with rows adding up to one:

$$\mathbf{\Gamma} = \begin{pmatrix} \gamma_{00\dots 0,00\dots 0} & \gamma_{00\dots 0,00\dots 1} & \dots & \gamma_{00\dots 0,11\dots 1} \\ \gamma_{00\dots 1,00\dots 0} & \gamma_{00\dots 1,00\dots 1} & \dots & \gamma_{00\dots 1,11\dots 1} \\ \vdots & \vdots & \ddots & \vdots \\ \gamma_{11\dots 1,00\dots 0} & \gamma_{11\dots 1,00\dots 1} & \dots & \gamma_{11\dots 1,11\dots 1} \end{pmatrix} \text{ with } \mathbf{\Gamma} \mathbf{1}^\top = \mathbf{1}^\top \quad (17)$$

In this paper we compare models using the independent copula, Frank copula, Gaussian factor copula and the general-dependent model. The copula models can be considered with shared or separate strain transition probabilities. The properties of the models that we have described are summarised in Table 1.

Table 1: Summary of models used in this study

Model type	Marginal transition	Joint transition	Number of transition parameters
No epidemic	Nil	Nil	0
Independent 1	γ	Equation 9	2
Independent 2	$\gamma^{(k)}$	Equation 10	$2K$
Frank copula 1	γ	Equations 11 and 15	$2 + 1$
Frank copula 2	$\gamma^{(k)}$	Equations 11 and 16	$2K + 1$
Gaussian factor copula 1	γ	Equations 13 and 15	$2 + K$
Gaussian factor copula 2	$\gamma^{(k)}$	Equations 13 and 16	$2K + K$
General-dependent	Nil	Equation 17	$2^K(2^K - 1)$

2.3 Inference

Let the parameters be denoted $\theta = (\mathbf{r}_{1:T}, \mathbf{s}_{1:C}, \mathbf{u}_{1:I}, \kappa_r, \kappa_s, \kappa_u, \mathbf{a}_{1:K}, \boldsymbol{\beta}_{1:K}, \boldsymbol{\Gamma})$, then the target posterior distribution can be decomposed using Bayes' theorem as:

$$\begin{aligned} \mathbb{P}(\theta | \mathbf{y}_{1:I,1:T,1:K}) &\propto \mathbb{P}(\mathbf{y}_{1:I,1:T,1:K} | \theta) \times \mathbb{P}(\theta) \\ &\propto \mathbb{P}(\theta) \prod_{i=1}^I \mathbb{P}(\mathbf{y}_{i,1:T,1:K} | \theta) \end{aligned} \quad (18)$$

using conditional independence between locations given \mathbf{u} .

2.3.1 Likelihood via forward filtering

Define the joint state space, $\mathcal{X} = \{0, 1\}^K$ for the joint Markov chain $\mathbf{x}_{i,1:T}$, and let $\theta_i = (\mathbf{r}, \mathbf{s}, u_i, \mathbf{a}, \boldsymbol{\beta}, \boldsymbol{\Gamma})$. We assume that the joint Markov chain starts from its stationary distribution, $\boldsymbol{\delta}$. Given the full joint transition probability matrix, $\boldsymbol{\Gamma}$, the stationary distribution is obtained by solving the linear system for $\boldsymbol{\delta}$ such that $\boldsymbol{\delta} = \boldsymbol{\delta}\boldsymbol{\Gamma}$ and $\boldsymbol{\delta}\mathbf{1}^\top = 1$ are both satisfied. The forward filtering algorithm [36] involves defining a sequence of vectors $\alpha_{i,t}$ with length $|\mathcal{X}|$, as follows:

$$\alpha_{i,t}(\mathbf{x}_{i,t}) = \mathbb{P}(\mathbf{y}_{i,1:t,1:K}, \mathbf{x}_{i,t} | \theta_i), \quad (19)$$

for each $\mathbf{x}_{i,t} \in \mathcal{X}$. For the initial timepoint we have:

$$\begin{aligned} \alpha_{i,1}(\mathbf{x}_{i,1}) &= \mathbb{P}(\mathbf{y}_{i,1,1:K}, \mathbf{x}_{i,1} | \theta_i) \\ &= \mathbb{P}(\mathbf{y}_{i,1,1:K} | \mathbf{x}_{i,1}, \theta_i) \mathbb{P}(\mathbf{x}_{i,1} | \theta_i) \\ &= \left(\prod_{k=1}^K \mathbb{P}(y_{i,1,k} | \mathbf{x}_{i,1}, \theta_i) \right) \delta_{\mathbf{x}_{i,1}}. \end{aligned}$$

For $t > 1$ these forward vectors satisfy the recursion:

$$\begin{aligned} \alpha_{i,t}(\mathbf{x}_{i,t}) &= \sum_{\mathbf{x}_{i,t-1} \in \mathcal{X}} \mathbb{P}(\mathbf{y}_{i,1:t,1:K}, \mathbf{x}_{i,t}, \mathbf{x}_{i,t-1} | \theta_i), \\ &= \sum_{\mathbf{x}_{i,t-1} \in \mathcal{X}} \mathbb{P}(\mathbf{y}_{i,t,1:K} | \mathbf{x}_{i,t}, \mathbf{y}_{i,1:t-1,1:K}, \mathbf{x}_{i,t-1}, \theta_i) \mathbb{P}(\mathbf{x}_{i,t} | \mathbf{y}_{i,1:t-1,1:K}, \mathbf{x}_{i,t-1}, \theta_i) \mathbb{P}(\mathbf{y}_{i,1:t-1,1:K}, \mathbf{x}_{i,t-1} | \theta_i) \\ &= \sum_{\mathbf{x}_{i,t-1} \in \mathcal{X}} \left(\prod_{k=1}^K \mathbb{P}(y_{i,t,k} | \mathbf{x}_{i,t}, \theta_i) \right) \mathbb{P}(\mathbf{x}_{i,t} | \mathbf{x}_{i,t-1}, \theta_i) \alpha_{i,t-1}(\mathbf{x}_{i,t-1}) \end{aligned}$$

The likelihood terms in Equation 18 can then be calculated as:

$$\mathbb{P}(\mathbf{y}_{i,1:T,1:K} | \theta) = \sum_{\mathbf{x}_{i,T} \in \mathcal{X}} \alpha_{i,T}(\mathbf{x}_{i,T}).$$

2.3.2 Marginal probability of an epidemic

The epidemic indicators in the spatio-temporal component, $\mathbf{x}_{i,t} = (x_{i,t,1}, \dots, x_{i,t,K})$, represent when and where an epidemic is occurring jointly across strains, where $x_{i,t,k} = 0$ indicates the endemic state and $x_{i,t,k} = 1$ indicates

the epidemic state. Hence, the probability of an epidemic can be obtained by local decoding using the backward part of the forward filtering backward sampling algorithm [36]. We are interested in the conditional probability $\mathbb{P}(\mathbf{x}_{i,t}|\mathbf{y}_{i,1:T,1:K}, \boldsymbol{\theta}_i)$, for each $t = 1, \dots, T$.

We define a sequence of T backward vectors, each with length $|\mathcal{X}| = 2^K$:

$$\beta_{i,t}(\mathbf{x}_{i,t}) = \mathbb{P}(\mathbf{y}_{i,(t+1):T,1:K}|\mathbf{x}_{i,t}, \boldsymbol{\theta}_i). \quad (20)$$

In particular we have:

$$\beta_{i,T}(\mathbf{x}_{i,T}) = \mathbb{P}(\Omega|\mathbf{x}_{i,T}, \boldsymbol{\theta}_i) = 1.$$

For $t = T - 1, \dots, 1$, the backward vectors satisfy the recursion:

$$\begin{aligned} \beta_{i,t-1}(\mathbf{x}_{i,t-1}) &= \mathbb{P}(\mathbf{y}_{i,t:T,1:K}|\mathbf{x}_{i,t-1}, \boldsymbol{\theta}_i) \\ &= \sum_{\mathbf{x}_{i,t} \in \mathcal{X}} \mathbb{P}(\mathbf{y}_{i,t:T,1:K}|\mathbf{x}_{i,t}, \boldsymbol{\theta}_i) \mathbb{P}(\mathbf{x}_{i,t}|\mathbf{x}_{i,t-1}, \boldsymbol{\theta}_i) \\ &= \sum_{\mathbf{x}_{i,t} \in \mathcal{X}} \mathbb{P}(\mathbf{y}_{i,(t+1):T,1:K}|\mathbf{x}_{i,t}, \boldsymbol{\theta}_i) \mathbb{P}(\mathbf{y}_{i,t,1:K}|\mathbf{x}_{i,t}, \boldsymbol{\theta}_i) \mathbb{P}(\mathbf{x}_{i,t}|\mathbf{x}_{i,t-1}, \boldsymbol{\theta}_i) \\ &= \sum_{\mathbf{x}_{i,t} \in \mathcal{X}} \beta_{i,t}(\mathbf{x}_{i,t}) \left(\prod_{k=1}^K \mathbb{P}(y_{i,t,k}|\mathbf{x}_{i,t}, \boldsymbol{\theta}_i) \right) \mathbb{P}(\mathbf{x}_{i,t}|\mathbf{x}_{i,t-1}, \boldsymbol{\theta}_i). \end{aligned}$$

With the forward α_t and backward β_t vectors defined as Equations 19 and 20 we can compute the marginal probability of an epidemic for each location and date:

$$\begin{aligned} \mathbb{P}(\mathbf{x}_{i,t}|\mathbf{y}_{i,1:T,1:K}, \boldsymbol{\theta}_i) &= \frac{\mathbb{P}(\mathbf{y}_{i,1:T,1:K}, \mathbf{x}_{i,t}|\boldsymbol{\theta}_i)}{\mathbb{P}(\mathbf{y}_{i,1:T,1:K}|\boldsymbol{\theta}_i)} \\ &= \frac{\mathbb{P}(\mathbf{y}_{i,1:t,1:K}, \mathbf{x}_{i,t}|\boldsymbol{\theta}_i) \mathbb{P}(\mathbf{y}_{i,(t+1):T,1:K}|\mathbf{x}_{i,t}, \mathbf{y}_{i,1:t}, \boldsymbol{\theta}_i)}{\mathbb{P}(\mathbf{y}_{i,1:T,1:K}|\boldsymbol{\theta}_i)} \\ &= \frac{\alpha_{i,t}(\mathbf{x}_{i,t}) \beta_{i,t}(\mathbf{x}_{i,t})}{\sum_{\mathbf{x}_{i,T} \in \mathcal{X}} \alpha_{i,T}(\mathbf{x}_{i,T})}. \end{aligned}$$

2.3.3 Missing and untyped data

In many real-world applications, statistical inference is often complicated by the presence of missing data. The methodology presented in this paper and its accompanying R package (MultiOutbreaks) deal with scenarios of missing data by replacing the corresponding emission density in Sections 2.3.1 and 2.3.2 with 1 for all states when data are missing. This is implemented under the assumption that the data are missing at random (MAR); see Section 2.3.4 in [36] and [37]. Similarly, there can be rare occasions of untyped data (that is, the overall incidence count is available, but no information on how it is distributed between strains). This is dealt with by summing the risks across all strains to evaluate the likelihood of the untyped incidence count, as done in previous studies [38].

2.3.4 Priors

Here we provide details and justifications for all prior distributions used for inference in the subsequent sections. For the transition probabilities in the independent and copula-dependent models, a Beta(1, 11) was chosen for the transition probability from the endemic to the epidemic state (p) to express a relatively low belief in such transitions. This prior has a monotonically decreasing density with one epidemic a year on average per strain, so that the model is conservatively using the epidemic state to prevent false positives. A Beta(6, 6) was chosen for the transition probability from the epidemic to the endemic state (q) to express a 0.5 probability of such transitions on average and therefore an average epidemic period of 2 months. For the general-dependent model, we chose a Dirichlet prior distribution $\text{Dir}(v_{i,0}, \dots, v_{i,2^K-1})$, $i \in \{0, \dots, 2^K - 1\}$, for each simplex in the full transition probability matrix (Equation 17) based on the marginal priors on p and q from the copula models. The parameters of the Dirichlet are derived by matching the expectation of the independent models to the general-dependent model, such that $(v_{i,0}, \dots, v_{i,2^K-1}) = \frac{1}{12} \times (\mathbb{E}[\Gamma_{i,0}], \dots, \mathbb{E}[\Gamma_{i,2^K-1}])$, with $\Gamma_{i,j}$ as defined in Equation 9. In the Frank copula with $K = 2$, a Normal(0, 100) prior was chosen for ψ , and for $K > 2$, an Exponential(0.5) prior was chosen. In the Gaussian factor copula, we placed a flat Uniform(-1, 1) prior on the factor loadings. The prior distribution for each

strain-specific epidemic effect (β_k) is a Gamma(2, 2) distribution which prevents label switching issues and ensures that the epidemic periods correspond to periods of strictly increased risk. These priors also facilitate a fair model comparison between all models in Table 1, see [39]. An informative prior $\text{Gamma}\left(0.01, \frac{0.01}{\exp(-15)}\right)$ was assumed for the transformed strain-specific intercept parameters $\phi_k = \exp(a_k)$ to allow a Gibbs-inspired proposal distribution during MCMC sampling. Following previous work [27], the trend, seasonal and spatial components have prior densities as specified in Equations A1, A2, and A3 respectively. These three priors are defined in terms of the precision parameters κ_r , κ_s and κ_u for the trend component, seasonal component and spatial component, respectively. The hyper-priors of these three hyper-parameters are Gamma(1, 0.0001), Gamma(1, 0.001) and Gamma(1, 0.01), respectively.

2.3.5 Monte Carlo sampling from the posterior

The target posterior of our model is a high-dimensional probability density with strongly correlated temporal components. Gradient-based Markov chain Monte Carlo (MCMC) methods such as Hamiltonian Monte Carlo (HMC) [40, 41] or Metropolis adjusted Langevin algorithm (MALA) [42, 43] are known to have significant success in sampling efficiently from these kinds of probability densities, compared to traditional MCMC sampling methods. This is due to their ability to initiate ambitious moves within the state space whilst maintaining reasonable acceptance rates through the use of local problem-specific information.

If $\theta \in \mathbb{R}^D$ with density $p(\theta)$ and log-density $\mathcal{L}(\theta) = \log p(\theta)$, then MALA uses a discrete approximation to the Langevin diffusion which satisfies the following stochastic differential equation:

$$d\theta(t) = \frac{1}{2} \nabla_{\theta} \mathcal{L}(\theta(t)) dt + dB(t), \quad (21)$$

where $B(t)$ is a D -dimensional Brownian motion. The first-order Euler–Maruyama discretization of the continuous-time process yields a tractable discrete-time approximation of the form:

$$\theta^* = \theta^n + \frac{\varepsilon^2}{2} \nabla_{\theta} \mathcal{L}(\theta^n) + \varepsilon z^n \quad (22)$$

where $z \sim \mathcal{N}(\mathbf{0}, \mathbf{I})$ and ε is the step size. The Metropolis accept-reject step [44, 45] is then incorporated to correct for the error introduced by the step size ε , thus guaranteeing convergence to the correct invariant measure.

The gradient-based MCMC method described above converges to the desired stationary distribution more rapidly than the popular random-walk MCMC algorithm. However, MALA can still face shortcomings when sampling high-dimensional targets with strongly correlated parameters such as the second-order random walk used as the trend component in our model (Equation 5). To address these shortcomings, a more efficient proposal is derived by noting that the space of parameterized probability density functions is endowed with a natural Riemann geometry [29]. The Riemannian manifold MALA (MMALA) proceeds by defining the Langevin diffusion having an invariant measure $p(\theta)$, $\theta \in \mathbb{R}^D$ directly on the Riemann manifold with arbitrary metric tensor $G(\theta)$. It was deduced that for a manifold with constant curvature, the position-specific preconditioned MALA proposal reduces to

$$\theta^* = \theta^n + \frac{\varepsilon^2}{2} G^{-1}(\theta^n) \nabla_{\theta} \mathcal{L}(\theta^n) + \varepsilon \sqrt{G^{-1}(\theta^n)} z^n, \quad (23)$$

with the Metropolis accept-reject step to ensure convergence to the target measure. We implement MMALA to update the temporal and spatial components of the model (r , s , and u). The precision parameters (κ_r , κ_s , and κ_u) were sampled from their full conditional distributions, exploiting the conjugacy between their hyper-priors and the likelihood of the temporal and spatial components. The strain-specific intercepts (a_k) were sampled using Gibbs-inspired moves as described in Section 2.3.6. The strain-specific regression parameters were each updated using simple Metropolis random walk moves with the proposal $\beta_{n+1} \sim \mathcal{N}(\beta_n, \sigma_{\beta}^2)$. The transition probabilities in the off-diagonals of γ in each of the independent and copula models were sampled using simple random walk moves. The copula parameter of the Frank copula models (ψ) is also updated using simple random walk moves. The copula parameters in the Gaussian factor copula model $\xi_{k,1} \in (-1, 1)$ were each transformed to $z_k \in \mathbb{R}$ using a probit-type transformation $z_k = \Phi^{-1}\left(\frac{\xi_{k,1}+1}{2}\right)$ and then updated using simple Metropolis random walk moves as previously described, with the Jacobian correction $2\phi(z)$, where Φ^{-1} and ϕ represent the inverse cumulative distribution function and the probability density function of a standard Gaussian distribution, respectively. We impose an identifiability constraint by fixing $\xi_{1,1} \approx 1$ since the factor model is invariant under global sign swapping, rotation, or scaling [46]. All simple random walk updates were implemented together with a Robbins-Monro adaptive tuning of the proposal standard deviations using the optimal high-dimensional target acceptance rate of 0.234 [47]. Each row of the transition probability matrix Γ in the general-dependent model was updated using Adaptive Dirichlet random-walk moves [38, 48] with a Dirichlet

proposal $\Gamma_{n+1}^{(i)} \sim \text{Dir}\left(v_{i,0}, \dots, v_{i,2^k-1} + h_n^{(i)} \Gamma_n^{(i)}\right)$, $i \in \{0, \dots, 2^k - 1\}$, where $\left(h_n^{(i)}\right)$ is used to adaptively tune the proposal to stabilize the acceptance rate at roughly 25%. After initializing $\log\left(h_1^{(i)}\right) = 0$, the subsequent tuning for $\log\left(h_n^{(i)}\right)$ is given by $\log\left(h_n^{(i)}\right) = \log\left(h_{n-1}^{(i)}\right) - 3$ if a proposed move is accepted or $\log\left(h_n^{(i)}\right) = \log\left(h_{n-1}^{(i)}\right) + 1$ if a proposed move is rejected. Finally, we use an adaptive Metropolis-Hastings random walk move with a multivariate Gaussian proposal and Robbins-Monro tuning [47, 49, 50] for an additional joint update of the strain-specific intercepts and regression parameters, transition probabilities (with logit transformation), and copula parameters (with probit-type transformation for the factor loadings) with the appropriate Jacobian corrections included. The second option provided in our *R* package is the dynamic HMC sampler via *cmdstanr*, an *R* interface to Stan [51]. This implementation offers the option to accelerate computations through a graphics processing unit (GPU) when available.

2.3.6 Gibbs-inspired update for strain-specific intercepts

The construction of an efficient proposal distribution is fundamental to the performance of a MCMC sampling algorithm. Here, we derive an approximate Gibbs conditional distribution as a proposal to update the strain-specific intercept parameters a_k within our MCMC scheme leveraging the Poisson-Gamma conjugacy. Define $\phi_k = \exp(a_k)$, and $\mu_{itk} = r_t + s_{t \bmod C} + u_i + x_{itk}\beta_k$. We can then rewrite Equation 4 as:

$$\begin{aligned} y_{itk} | \phi_k, \mu_{itk}, e_{it} &\sim \text{Poisson}(e_{it} \phi_k \exp(\mu_{itk})) \\ \mathbf{P}(y_{1:I,1:T,k} | \phi_k, \mu_{itk}, e_{it}) &= \prod_{i=1}^I \prod_{t=1}^T \frac{(e_{it} \phi_k \exp(\mu_{itk}))^{y_{itk}}}{y_{itk}!} \exp(-e_{it} \phi_k \exp(\mu_{itk})) \\ &= \left[\prod_{i=1}^I \prod_{t=1}^T \frac{(e_{it} \exp(\mu_{itk}))^{y_{itk}}}{y_{itk}!} \right] \left[\phi_k^{\sum_{i=1}^I \sum_{t=1}^T y_{itk}} \exp\left(-\phi_k \sum_{i=1}^I \sum_{t=1}^T e_{it} \exp(\mu_{itk})\right) \right] \\ \mathbf{P}(y_{1:I,1:T,k} | \phi_k, \mu_{itk}, e_{it}) &\propto \phi_k^{\mathbf{Y}_k} \exp(-\phi_k \mathbf{S}_k) \end{aligned}$$

where $\mathbf{Y}_k = \sum_{i=1}^I \sum_{t=1}^T y_{itk}$, and $\mathbf{S}_k = \sum_{i=1}^I \sum_{t=1}^T e_{it} \exp(\mu_{itk})$.

Conjugacy can therefore be achieved by assuming a prior $\phi_k \sim \text{Gamma}(\alpha_k^\phi, \beta_k^\phi)$ which leads to the full conditional distribution:

$$\phi_k | y_{1:I,1:T,k}, \mathbf{x}, \mu_{itk}, e_{1:I,1:T} \sim \text{Gamma}(\alpha_k^\phi + \mathbf{Y}_k, \beta_k^\phi + \mathbf{S}_k)$$

Given that the joint-state sequence \mathbf{x} are not directly observable from data, we smooth \mathbf{S}_k using the marginal posterior probabilities of the hidden states, and marginalize over the state space \mathcal{X} to obtain an unbiased estimate $\hat{\mathbf{S}}_k$ for the pseudo-Gibbs sampler. A Metropolis-Hastings accept-reject step with the Jacobian of transformation $\exp(a_k)$ is incorporated to guaranty targetting of the correct stationary distribution.

2.3.7 Gradients and metric tensor for MMALA

Here, we consider the gradients and metric tensor required for inference. The choice of metric tensor for our MMALA implementation is the observed Fisher information matrix of the log posterior $\mathbf{G}(\boldsymbol{\theta}) = -\mathbf{H}(\boldsymbol{\theta})$, where $\mathbf{H}(\boldsymbol{\theta})$ is the Hessian matrix of the log posterior. By the linearity property of differentiation, the gradients and Hessian of the log posterior with respect to $\boldsymbol{\theta}$ satisfy the following:

$$\begin{aligned} \nabla_{\boldsymbol{\theta}} \log \mathbf{P}(\boldsymbol{\theta} | y_{1:I,1:T,1:K}) &= \nabla_{\boldsymbol{\theta}} \log \mathbf{P}(y_{1:I,1:T,1:K} | \boldsymbol{\theta}) + \nabla_{\boldsymbol{\theta}} \log \mathbf{P}(\boldsymbol{\theta}). \\ \nabla_{\boldsymbol{\theta}}^2 \log \mathbf{P}(\boldsymbol{\theta} | y_{1:I,1:T,1:K}) &= \nabla_{\boldsymbol{\theta}}^2 \log \mathbf{P}(y_{1:I,1:T,1:K} | \boldsymbol{\theta}) + \nabla_{\boldsymbol{\theta}}^2 \log \mathbf{P}(\boldsymbol{\theta}). \end{aligned}$$

Since the joint-state sequence \mathbf{x} has been marginalized out as described in Section 2.3.1, we now require gradients and Hessian from the log marginal likelihood and the log prior. Exact methods to directly propagate the gradients and Hessian from the log marginal likelihood within the forward algorithm described in Section 2.3.1 have been proposed [52, 53, 54], however, these methods would be computationally intensive in the models being introduced in this paper since model parameters follow the temporal and spatial dimensions of the data being analyzed. In particular, direct propagation of the Hessian within the forward algorithm requires a heavy multi-dimensional array which is practically infeasible in our setting. To obtain a computationally efficient approach that still preserves exact Bayesian posterior inference, we exploit the Fisher and Louis identities.

2.3.8 The Fisher and Louis identities

In many statistical models involving latent variables, evaluating the gradients and the Hessian matrix from the complete-data log likelihood is often complicated by the unobserved latent variables. The Fisher and Louis identities provide a theoretical basis for computing the gradients and the Hessian matrix directly from the incomplete-data log likelihood, respectively. For a more detailed discussion and proof of these identities, see [55] and Section D.2 of [56]. The following Equations 24 and 25 are the Fisher and Louis identities, respectively. These identities relate the gradients and Hessian of the incomplete-data log likelihood to the complete-data log likelihood.

$$\nabla_{\theta} \log \mathbb{P}(\mathbf{y}|\theta) = \sum_{x \in \mathcal{X}} \{\nabla_{\theta} \log \mathbb{P}(x, \mathbf{y}|\theta)\} \mathbb{P}(x|\mathbf{y}, \theta) = \mathbb{E}_{x|\mathbf{y}, \theta} [\nabla_{\theta} \log \mathbb{P}(x, \mathbf{y}|\theta)]. \quad (24)$$

$$\begin{aligned} \nabla_{\theta}^2 \log \mathbb{P}(\mathbf{y}|\theta) &= \sum_{x \in \mathcal{X}} [\nabla_{\theta}^2 \log \mathbb{P}(x, \mathbf{y}|\theta) + \{\nabla_{\theta} \log \mathbb{P}(x, \mathbf{y}|\theta)\} \{\nabla_{\theta} \log \mathbb{P}(x, \mathbf{y}|\theta)\}^{\top}] \mathbb{P}(x|\mathbf{y}, \theta) \\ &\quad - \{\nabla_{\theta} \log \mathbb{P}(\mathbf{y}|\theta)\} \{\nabla_{\theta} \log \mathbb{P}(\mathbf{y}|\theta)\}^{\top} \\ &= \mathbb{E}_{x|\mathbf{y}, \theta} [\nabla_{\theta}^2 \log \mathbb{P}(x, \mathbf{y}|\theta) + \{\nabla_{\theta} \log \mathbb{P}(x, \mathbf{y}|\theta)\} \{\nabla_{\theta} \log \mathbb{P}(x, \mathbf{y}|\theta)\}^{\top}] \\ &\quad - \{\nabla_{\theta} \log \mathbb{P}(\mathbf{y}|\theta)\} \{\nabla_{\theta} \log \mathbb{P}(\mathbf{y}|\theta)\}^{\top}. \end{aligned} \quad (25)$$

2.3.9 Decomposing the complete-data log likelihood in the Fisher and Louis identities

The complete-data log likelihood can be decomposed as:

$$\log \mathbb{P}(\mathbf{y}, \mathbf{x}|\theta) = \log \mathbb{P}(\mathbf{y}|\mathbf{x}, \theta) + \log \mathbb{P}(\mathbf{x}|\theta), \quad (26)$$

and inserting this into the Fisher identity implies:

$$\begin{aligned} \nabla_{\theta} \log \mathbb{P}(\mathbf{y}|\theta) &= \mathbb{E}_{x|\mathbf{y}, \theta} [\nabla_{\theta} \log \mathbb{P}(\mathbf{y}|\mathbf{x}, \theta) + \nabla_{\theta} \log \mathbb{P}(\mathbf{x}|\theta)] \\ &= \mathbb{E}_{x|\mathbf{y}, \theta} [\nabla_{\theta} \log \mathbb{P}(\mathbf{y}|\mathbf{x}, \theta)] + \mathbb{E}_{x|\mathbf{y}, \theta} [\nabla_{\theta} \log \mathbb{P}(\mathbf{x}|\theta)]. \end{aligned} \quad (27)$$

Similarly, the Louis identity implies:

$$\begin{aligned} \nabla_{\theta}^2 \log \mathbb{P}(\mathbf{y}|\theta) &= \sum_{x \in \mathcal{X}} (\nabla_{\theta}^2 \log \mathbb{P}(\mathbf{y}|\mathbf{x}, \theta) + \nabla_{\theta}^2 \log \mathbb{P}(\mathbf{x}|\theta)) \mathbb{P}(x|\mathbf{y}, \theta) \\ &\quad + \sum_{x \in \mathcal{X}} (\{\nabla_{\theta} \log \mathbb{P}(\mathbf{y}|\mathbf{x}, \theta) + \nabla_{\theta} \log \mathbb{P}(\mathbf{x}|\theta)\} \{\nabla_{\theta} \log \mathbb{P}(\mathbf{y}|\mathbf{x}, \theta) + \nabla_{\theta} \log \mathbb{P}(\mathbf{x}|\theta)\}^{\top}) \mathbb{P}(x|\mathbf{y}, \theta) \\ &\quad - \{\nabla_{\theta} \log \mathbb{P}(\mathbf{y}|\theta)\} \{\nabla_{\theta} \log \mathbb{P}(\mathbf{y}|\theta)\}^{\top}. \end{aligned}$$

2.3.10 Analytic gradients and Hessian of the log likelihood

Recall the general form of our model in Equation 3. The complete-data log likelihood in the context of our model is written as:

$$\begin{aligned} \log \mathbb{P}(\mathbf{y}_{1:L,1:T,1:K}, \mathbf{x}|\theta) &= \sum_{i=1}^I \sum_{t=1}^T \sum_{k=1}^K \{y_{itk}(a_k + r_t + s_{t \bmod C} + u_i + x_{itk}\beta_k) - \exp(a_k + r_t + s_{t \bmod C} + u_i + x_{itk}\beta_k)e_{it} \\ &\quad + y_{itk} \log e_{it} - \log y_{itk}!\} + \log \mathbb{P}(\mathbf{x}|\Gamma), \end{aligned} \quad (28)$$

where we have used the fact that, in the prior, the joint-state sequence \mathbf{x} is conditionally independent of all components of θ except for Γ , and so $\mathbb{P}(\mathbf{x}|\theta) = \mathbb{P}(\mathbf{x}|\Gamma)$. Now differentiating this complete-data log likelihood with respect to r_t , $s_{t \bmod C}$, and u_i gives:

$$\begin{aligned} \nabla_{r_t} \log \mathbb{P}(\mathbf{y}_{1:L,1:T,1:K}, \mathbf{x}|\theta) &= \sum_{i=1}^I \sum_{k=1}^K \{y_{itk} - \exp(a_k + r_t + s_{t \bmod C} + u_i + x_{itk}\beta_k)e_{it}\} \\ \nabla_{s_{t \bmod C}} \log \mathbb{P}(\mathbf{y}_{1:L,1:T,1:K}, \mathbf{x}|\theta) &= \sum_{t: t \bmod C = c} \sum_{i=1}^I \sum_{k=1}^K \{y_{itk} - \exp(a_k + r_t + s_{t \bmod C} + u_i + x_{itk}\beta_k)e_{it}\} \\ \nabla_{u_i} \log \mathbb{P}(\mathbf{y}_{1:L,1:T,1:K}, \mathbf{x}|\theta) &= \sum_{t=1}^T \sum_{k=1}^K \{y_{itk} - \exp(a_k + r_t + s_{t \bmod C} + u_i + x_{itk}\beta_k)e_{it}\}, \end{aligned}$$

respectively. To apply the Fisher and Louis identities, we define η_{itk} as the following posterior expectation, where we smooth $e_{it}\lambda_{itk}$ and marginalize over the state space \mathcal{X} :

$$\eta_{itk} := \mathbb{E}_{\mathbf{x}|y_{1:L,1:T,1:K},\boldsymbol{\theta}} [e_{it}\lambda_{itk}] = \sum_{\mathbf{x}_{it} \in \mathcal{X}} e_{it} \exp(a_k + r_t + s_{t \bmod C} + u_i + x_{itk}\beta_k) \mathbb{P}(\mathbf{x}_{it}|y_{i,1:T,1:K}, \boldsymbol{\theta}), \quad (29)$$

where $\mathbb{P}(\mathbf{x}_{it}|y_{i,1:T,1:K}, \boldsymbol{\theta})$ is obtained via the backward algorithm described in Section 2.3.2.

For a given timepoint t , the gradient of the log marginal likelihood with respect to the trend component r_t is given by:

$$\nabla_{r_t} \log \mathbb{P}(\mathbf{y}_{1:L,1:T,1:K}|\boldsymbol{\theta}) = \mathbb{E}_{\mathbf{x}|y_{1:L,1:T,1:K},\boldsymbol{\theta}} [\nabla_{r_t} \log \mathbb{P}(\mathbf{y}_{1:L,1:T,1:K}, \mathbf{x}|\boldsymbol{\theta})] = \sum_{i=1}^I \sum_{k=1}^K \{y_{itk} - \eta_{itk}\}.$$

For season c such that $c = t \bmod C$ for $t = 1, 2, \dots, T$, the gradient of the log marginal likelihood with respect to the seasonal component $s_{t \bmod C}$ is given by:

$$\nabla_{s_{t \bmod C}} \log \mathbb{P}(\mathbf{y}_{1:L,1:T,1:K}|\boldsymbol{\theta}) = \mathbb{E}_{\mathbf{x}|y_{1:L,1:T,1:K},\boldsymbol{\theta}} [\nabla_{s_{t \bmod C}} \log \mathbb{P}(\mathbf{y}_{1:L,1:T,1:K}, \mathbf{x}|\boldsymbol{\theta})] = \sum_{t:t \bmod C=c} \sum_{i=1}^I \sum_{k=1}^K \{y_{itk} - \eta_{itk}\}$$

For a given spatial location i , the gradient of the log marginal likelihood with respect to the spatial component u_i is given by:

$$\nabla_{u_i} \log \mathbb{P}(\mathbf{y}_{1:L,1:T,1:K}|\boldsymbol{\theta}) = \mathbb{E}_{\mathbf{x}|y_{1:L,1:T,1:K},\boldsymbol{\theta}} [\nabla_{u_i} \log \mathbb{P}(\mathbf{y}_{1:L,1:T,1:K}, \mathbf{x}|\boldsymbol{\theta})] = \sum_{t=1}^T \sum_{k=1}^K \{y_{itk} - \eta_{itk}\}.$$

Given that our chosen metric tensor is the observed Fisher information matrix $G(\boldsymbol{\theta}) = -H(\boldsymbol{\theta})$, we employ the expected curvature component of the Louis identity from the log marginal likelihood, which is a diagonal matrix given our model, to guaranty positive definiteness [29], together with the observed Fisher information matrix from the log prior density. This choice is practically and computationally desirable in our model because it ensures that the observed information matrix is sparse and positive definite, which offers fast matrix inversion.

$$\begin{aligned} \nabla_{\boldsymbol{\theta}}^2 \log \mathbb{P}(\mathbf{y}|\boldsymbol{\theta}) &\approx \sum_{\mathbf{x} \in \mathcal{X}} \nabla_{\boldsymbol{\theta}}^2 \log \mathbb{P}(\mathbf{y}, \mathbf{x}|\boldsymbol{\theta}) \mathbb{P}(\mathbf{x}|\mathbf{y}, \boldsymbol{\theta}) = \mathbb{E}_{\mathbf{x}|\mathbf{y},\boldsymbol{\theta}} [\nabla_{\boldsymbol{\theta}}^2 \log \mathbb{P}(\mathbf{y}|\mathbf{x}, \boldsymbol{\theta})] + \mathbb{E}_{\mathbf{x}|\mathbf{y},\boldsymbol{\theta}} [\nabla_{\boldsymbol{\theta}}^2 \log \mathbb{P}(\mathbf{x}|\boldsymbol{\theta})] \\ \nabla_{r_t}^2 \log \mathbb{P}(\mathbf{y}_{1:L,1:T,1:K}|\boldsymbol{\theta}) &\approx \mathbb{E}_{\mathbf{x}|y_{1:L,1:T,1:K},\boldsymbol{\theta}} [\nabla_{r_t}^2 \log \mathbb{P}(\mathbf{y}_{1:L,1:T,1:K}, \mathbf{x}|\boldsymbol{\theta})] = \sum_{i=1}^I \sum_{k=1}^K \{-\eta_{itk}\} \\ \nabla_{s_{t \bmod C}}^2 \log \mathbb{P}(\mathbf{y}_{1:L,1:T,1:K}|\boldsymbol{\theta}) &\approx \mathbb{E}_{\mathbf{x}|y_{1:L,1:T,1:K},\boldsymbol{\theta}} [\nabla_{s_{t \bmod C}}^2 \log \mathbb{P}(\mathbf{y}_{1:L,1:T,1:K}, \mathbf{x}|\boldsymbol{\theta})] = \sum_{t:t \bmod C=c} \sum_{i=1}^I \sum_{k=1}^K \{-\eta_{itk}\} \\ \nabla_{u_i}^2 \log \mathbb{P}(\mathbf{y}_{1:L,1:T,1:K}|\boldsymbol{\theta}) &\approx \mathbb{E}_{\mathbf{x}|y_{1:L,1:T,1:K},\boldsymbol{\theta}} [\nabla_{u_i}^2 \log \mathbb{P}(\mathbf{y}_{1:L,1:T,1:K}, \mathbf{x}|\boldsymbol{\theta})] = \sum_{t=1}^T \sum_{k=1}^K \{-\eta_{itk}\}. \end{aligned}$$

The cross-derivatives in the Hessians of $\log \mathbb{P}(\mathbf{y}_{1:L,1:T,1:K}|\boldsymbol{\theta})$ in each of \mathbf{r} and \mathbf{s} are all zeros since they are independent across time in the likelihood. Similarly for \mathbf{u} since they are all independent across space in the likelihood. The exact analytic gradients and Hessian for the temporal and spatial components from the log priors are provided in Appendix A.6.

2.3.11 Sum-to-zero constraints

The Intrinsic Gaussian Markov Random Fields (IGMRF) used as prior distributions for the trend, seasonal, and spatial components (Equations A1,A2, A3, respectively) are improper models and therefore require the sum-to-zero constraint for identifiability. The gradient-based MCMC method presented in this paper adopts the QR-decomposition approach, projecting the temporal and spatial components, their gradients, and their observed Fisher information matrices onto a lower-dimensional unconstrained space using the orthonormal sub-matrix $\mathbf{Q}_2 \in \mathbb{R}^{n \times n-1}$ obtained from \mathbf{Q} in the QR-decomposition with $\mathbf{Q} = [\mathbf{Q}_1, \mathbf{Q}_2]$, where $\mathbf{Q}_1 \in \mathbb{R}^{n \times 1}$ is the leftmost column vector in \mathbf{Q} , and the columns of \mathbf{Q}_2 span the null space of the constraint, that is, $\mathbf{Q}_2^T \mathbf{1} = \mathbf{0}$. This projection ensures that the reparameterized parameters live in an unconstrained lower-dimensional space, and that the original parameters satisfy the sum-to-zero constraint while

preserving the local geometric structure of the posterior distribution. Suppose we are interested in sampling θ while imposing the sum-to-zero constraint for identifiability,

$$\mathbf{1}^\top \theta = 0,$$

we define the unconstrained subset ϑ and reparameterize as follows:

$$\theta = Q_2 \vartheta,$$

where $\vartheta \in \mathbb{R}^{n-1}$ is unconstrained. Since Q_2 span the null space of the constraint, $\theta \in \mathbb{R}^n$ automatically satisfies the sum-to-zero constraint. The unconstrained parameters being sampled are ϑ , and the projected gradients are:

$$\nabla_{\vartheta} \mathcal{L}(\vartheta) = Q_2^\top \nabla_{\theta} \mathcal{L}(\theta).$$

The projected metric tensor is given by:

$$G(\vartheta) = Q_2^\top G(\theta) Q_2.$$

For a more detailed discussion about sampling on a constraint manifold, see [57].

2.4 Bayesian model comparison

Bayesian model comparison is typically carried out by computing the Bayes factor [58] which is the ratio of the model evidence $\mathbb{P}(\mathbf{y})$ from competing models, defined as:

$$\mathbb{P}(\mathbf{y}) = \int_{\Theta} \mathbb{P}(\mathbf{y}|\theta) \mathbb{P}(\theta) d\theta. \quad (30)$$

Here we consider two methods for evaluating the high dimensional integral in Equation 30 for our models: bridge sampling and importance sampling. Bridge sampling was originally introduced to directly compute the Bayes factor of two competing models [59, 58, 60]. However, this approach would not be efficient here as we have several competing models. Recent advances show that individual marginal likelihoods can be estimated directly using bridge sampling [61]. This involves the construction of a bridge function and the use of samples from both the proposal distribution and the posterior distribution. The importance sampling method, on the other hand, uses samples from the proposal distribution alone. It theoretically provides an unbiased estimate of the marginal likelihood [62], but its performance deteriorates in high dimension due to increasing variance. The bridge sampling approach deals with this variance problem through the use of a well-constructed bridge function [60]. Table 2 compares the key features of these two model comparison methods, where $\mathbb{P}(\mathbf{y}|\theta)$ is the likelihood, $\mathbb{P}(\theta)$ is the prior density, $g(\theta)$ is the proposal distribution, $h(\theta)$ is the bridge function, $\tilde{\theta}_i$ is the i -th sample from the proposal distribution $g(\theta)$, and θ_j^* is the j -th sample from the posterior distribution $\mathbb{P}(\theta|\mathbf{y})$. Note that for the bridge sampling method the bridge function $h(\theta)$ contains the quantity of interest $\mathbb{P}(\mathbf{y})$ and therefore implementation typically requires an iterative scheme. To this end we leverage the implementation from the R package *bridgesampling* [63], where we provide our custom log likelihood, log priors and the necessary parameter constraints.

Table 2: Comparison of methods to estimate marginal likelihood

Method	Estimator	Samples	Bridge function $h(\theta)$
Bridge sampling	$\frac{1}{N_2} \sum_{i=1}^{N_2} \frac{\mathbb{P}(\mathbf{y} \tilde{\theta}_i) \mathbb{P}(\tilde{\theta}_i) h(\tilde{\theta}_i)}{\frac{1}{N_1} \sum_{j=1}^{N_1} h(\theta_j^*) g(\theta_j^*)}$	$\tilde{\theta}_i \sim g(\theta)$	$h(\theta) \propto \left(\frac{N_1}{N_1+N_2} \mathbb{P}(\mathbf{y} \theta) \mathbb{P}(\theta) + \frac{N_2}{N_1+N_2} \mathbb{P}(\mathbf{y}) g(\theta) \right)^{-1}$
Importance sampling	$\frac{1}{N} \sum_{i=1}^N \frac{\mathbb{P}(\mathbf{y} \tilde{\theta}_i) \mathbb{P}(\tilde{\theta}_i)}{g(\tilde{\theta}_i)}$	$\tilde{\theta}_i \sim g(\theta)$	$h(\theta) = \frac{1}{g(\theta)}$

3 Simulation study

We performed a simulation study in order to assess the validity and scalability of the Bayesian inference methodology described above for each model specified in Table 1. We considered that there were five small cities each consisting of approximately 500,000 susceptible individuals on average, and four large cities each consisting of approximately one million susceptible individuals on average. The cities were located in such a way that two cities are considered neighbors if they share a common border. Figure S1 illustrates the adjacency structure of the hypothetical spatial locations being studied. Monthly data were simulated with each of the eight models using the joint state-space formulation specified in Equation 4 for a 5-year period at the nine different geographical locations for $K = 5$ strains. The parameters in the spatio-temporal epidemic components and the background per-strain intercepts used for the simulation study were as follows. The simulated intercept parameters for each strain were $a_1 = -13.18$, $a_2 = -12.31$, $a_3 = -12.49$, $a_4 = -13.64$ and $a_5 = -13.98$. The epidemic effects for each strain were $\beta_1 = 1.65$, $\beta_2 = 0.95$, $\beta_3 = 1.40$, $\beta_4 = 1.10$ and $\beta_5 = 1.70$. The Frank copula models used $\psi = 6.5$ whereas the Gaussian copula models used $\rho_{12} = 0.80$, $\rho_{13} = -0.85$, $\rho_{14} = 0.90$, $\rho_{15} = -0.80$, $\rho_{23} = -0.86$, $\rho_{24} = 0.87$, $\rho_{25} = -0.85$, $\rho_{34} = -0.80$, $\rho_{35} = 0.80$ and $\rho_{45} = -0.87$. Figure 2 shows the simulated incidence data for each strain, location and date, and for each of the eight models.

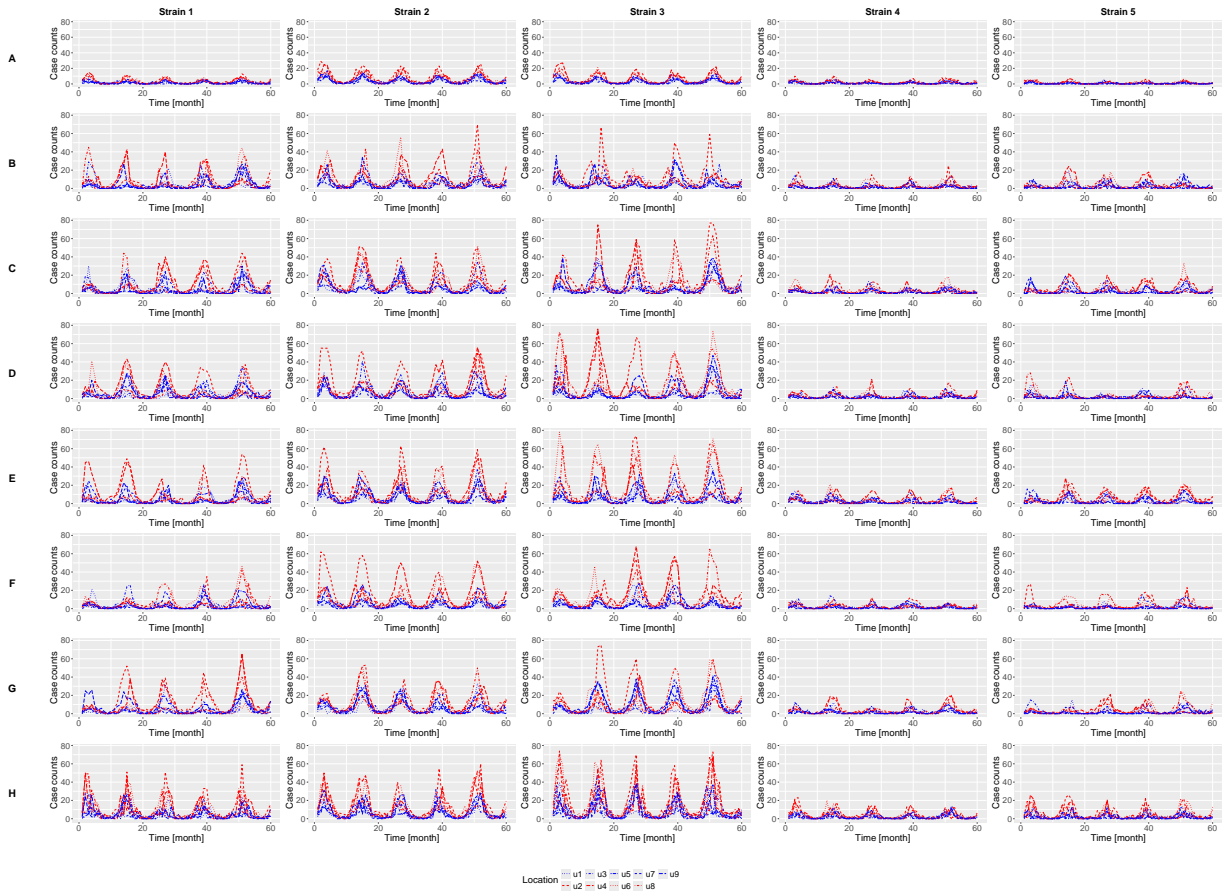


Figure 2: Multi-type model simulations with $K = 5$ strains from (A) No epidemic model (B) Independent 1 model (C) Independent 2 model (D) Frank copula 1 model (E) Frank copula 2 model (F) Frank copula 2 model (G) Gaussian factor copula 1 model (H) Gaussian factor copula 2 model, and (H) General-dependent model.

For each of these eight simulated datasets, we wanted to perform inference under the same model as was used for simulation. We tried the two approaches described previously: on one hand our purpose built approach combining use of MMALA, Gibbs-like and random-walk moves and on the other hand the generic approach implemented by the Stan inference engine. We found that the former is significantly faster than the latter, which can be explained by the fact that we provide analytical gradients and observed Fisher information matrices to the samplers in contrast to Stan where numerical gradients via *autodiff* are used. In comparison of computational costs, the total runtime using Stan's HMC

No-U-turn sampler with 4 parallel chains on a GPU to run 2000 iterations (1000 warm-up and 1000 sampling, target acceptance statistic $\delta = 0.95$) for the independent model 1 (Equation 9) was about 48 hours, as compared to 1.09 hours to run 50000 iterations using our purpose-built sampling methods, where major code bottlenecks have been written in C++. The total run time for the general-dependent model (Equation 17) was approximately 5.9 hours to obtain 50000 MCMC samples with our purpose-built approach, whereas Stan would not run in a reasonable amount of time. The remainder of this article will therefore focus on the use of our purpose-built approach.

Figure 3 compares the correct and inferred values of the temporal trend and seasonal components, for each of the eight runs. Likewise, Figure 4 shows the correct and inferred values of the spatial components, intercepts, epidemic effects, transition probabilities and copula parameters for each of the eight runs. For all parameters shown in Figures 3 and 4 we find that the inferred posterior mean is close to the correct value, and that the 95% credible interval almost always includes the correct value. Finally, Figure 5 shows the posterior probabilities of epidemics for each location, date and strain and for each of the seven models which allow epidemics. These probabilities are overall in excellent alignment with the correct epidemics that took place when simulating the data. There are a few examples where real epidemics have not been identified (false negatives), but this typically happens for epidemics lasting only one of a few months. Such short epidemics would not have had much impact on the data and therefore are expected to be more difficult to detect. There are even less instances of inferred epidemics when no real epidemic had happened (false positives) if we consider 50% posterior probability to be the cutoff for calling epidemics, and all of them had probabilities below 80%. The results are less clear for the general-dependent model (Figure 5G) due to the more frequent transitions between non-epidemic and epidemic states in this model. Nevertheless, and in spite of the high number of parameters in this model (with $K = 5$ strains there are 992 parameters in the transition matrix alone), inference is still satisfactory overall for this model.

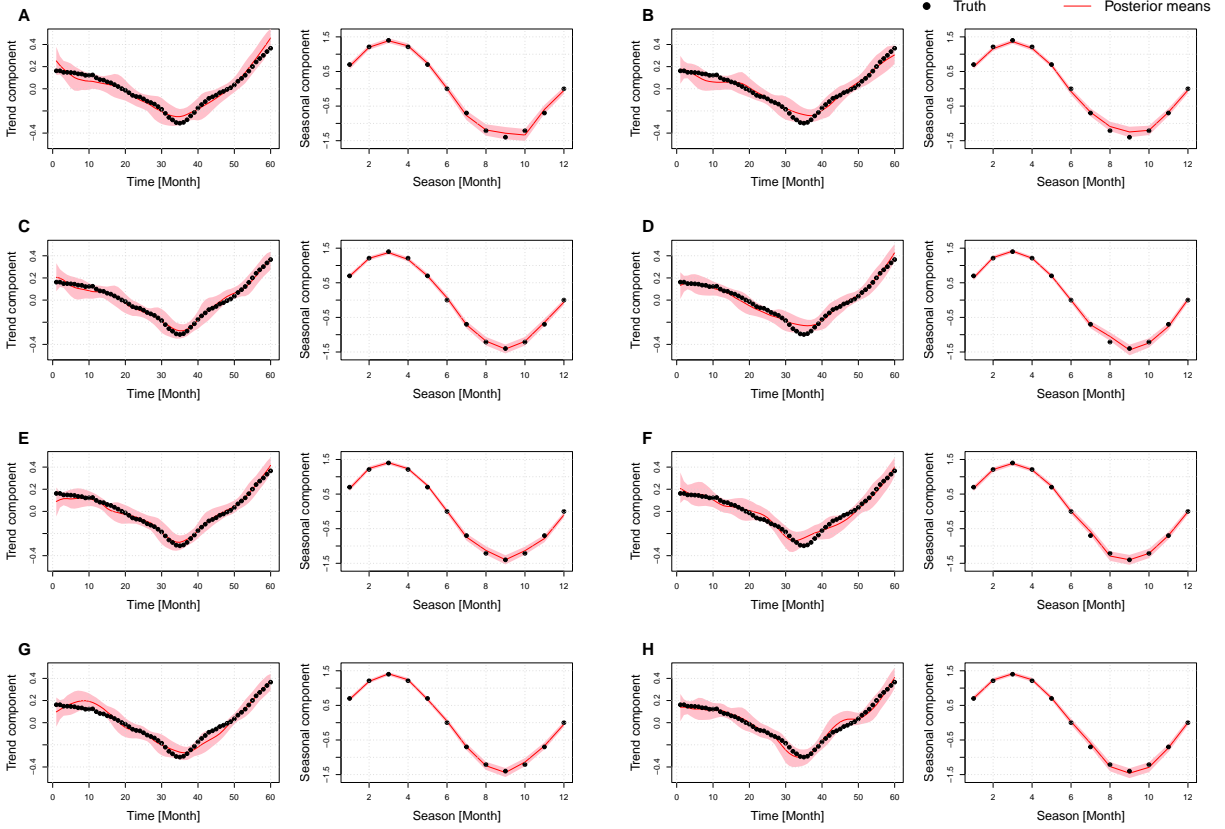


Figure 3: Posterior means, 95% credible intervals and the true values of the temporal trend and seasonal components from (A) No epidemic model (B) Independent 1 model (C) Independent 2 model (D) Frank copula 1 model (E) Frank copula 2 model (F) Gaussian factor copula 1 model (G) Gaussian factor copula 2 model, and (H) General-dependent model.

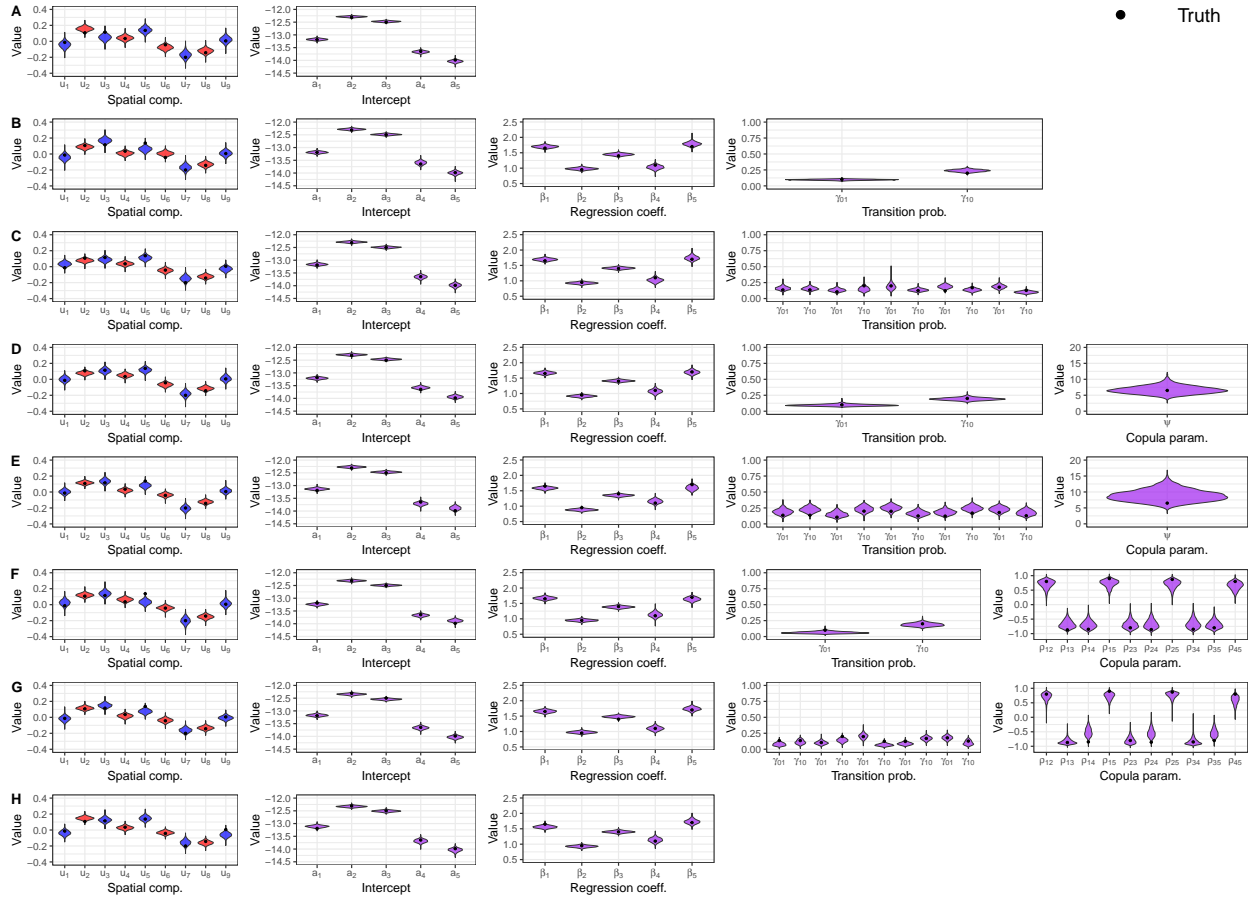


Figure 4: Posterior densities and the true values of the spatial components, intercepts, epidemic effects, transition probabilities and copula parameters from (A) No epidemic model (B) Independent 1 model (C) Independent 2 model (D) Frank copula 1 model (F) Frank copula 2 model (G) Gaussian factor copula 1 model (H) Gaussian factor copula 2 model, and (H) General-dependent model.

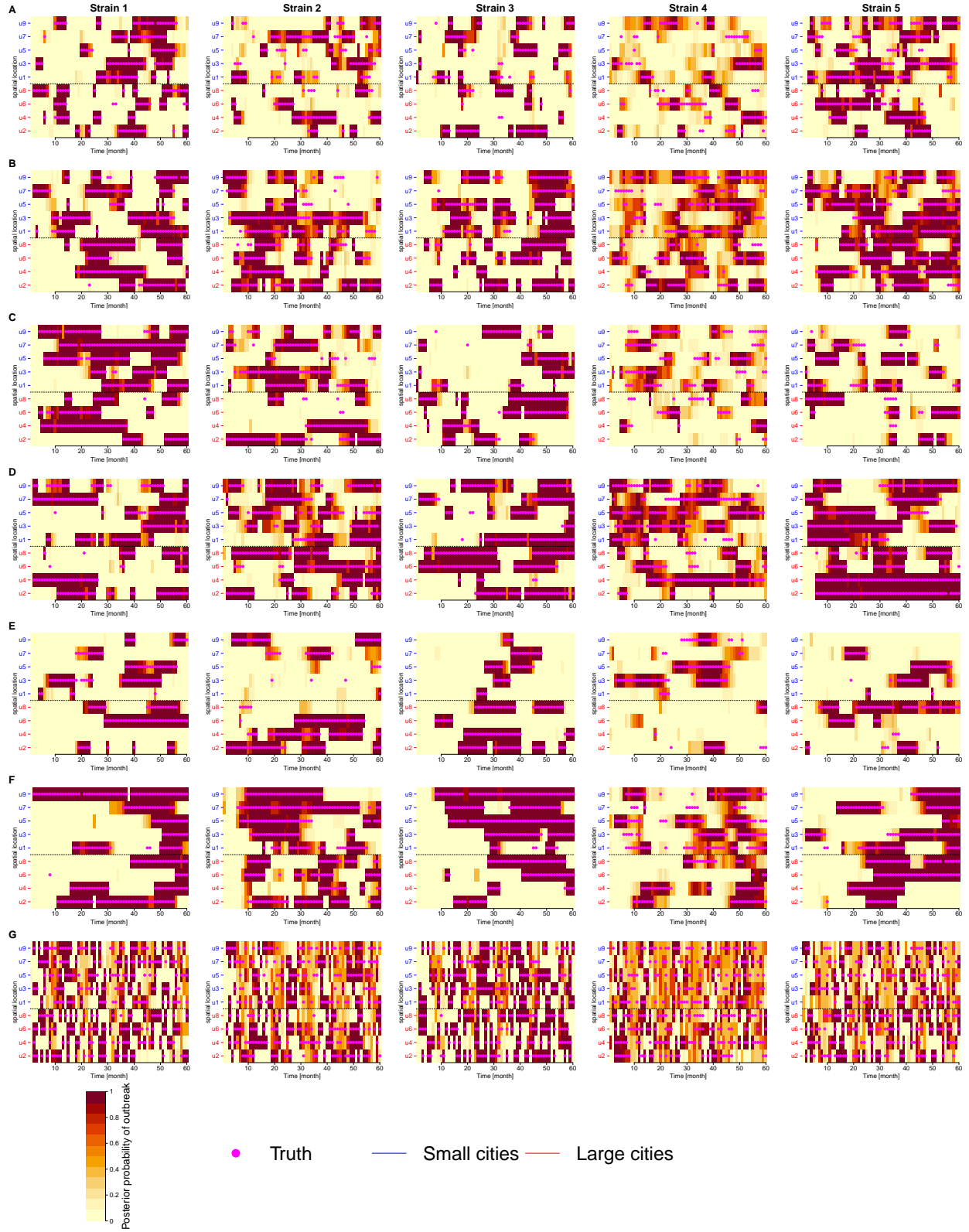


Figure 5: Heatmap showing simulated epidemics per strain and inferred probability of the epidemic state for strains 1 to 5 from (A) Independent 1 model (B) Independent 2 model (C) Frank copula 1 model (D) Frank copula 2 model (E) Gaussian factor copula 1 model (F) Gaussian factor copula 2 model, and (G) General-dependent model.

4 Application to multi-type invasive meningococcal disease

The European Center for Disease Prevention and Control (ECDC) publishes a Surveillance Atlas of Infectious Diseases which contains monthly incidence data on invasive meningococcal disease from 26 European countries [30]. The data were available up to December 2023, however, our analysis is restricted to the period from January 2010 to December 2019 to avoid possible confounding factors introduced first by the withdrawal of the United Kingdom (UK) from the European Union and then by the COVID-19 pandemic. Although the dataset includes some missing values, our methodology accommodates this under the assumption of data missing at random as discussed in Section 2.3.3. We considered $K = 4$ types corresponding to the major serogroups of *Neisseria meningitidis* B, W, Y and C [3]. The ECDC atlas also includes smaller numbers of cases for other serogroups (eg A, X and Z) which were excluded from the analysis. The raw data is shown in Figure S2, from which clear yearly seasonal patterns can be seen. It is also clear that the UK has a high number of disease cases for serogroups B, W and Y, even compared to other countries with a comparably large population such as Germany, France or Italy. This higher incidence may be due to better report rates and surveillance in the UK relative to the other countries, but we are unable to investigate this.

Annual population counts for each country were available from the Eurostat database [64]. To derive approximate monthly population counts, we apply linear interpolation to ensure that the population data align with the temporal resolution of the incidence records. Geographical data on the distances between the capitals of the countries included in our analysis were obtained from the Cshapes R package [65]. Leveraging this data, we classified countries as adjacent if the distance between their capitals was less than or equal to 820 km. This threshold was chosen to ensure that approximately 20% of pairs of countries were classified as neighbours, providing a balanced representation of geographical proximity in the analysis.

We performed Bayesian inference on this data separately under each of the eight models listed in Table 1. We run two MCMC chains for all fitted models, with 200000 iterations per chain. MCMC convergence and diagnostics were assessed using the coda R package [66] and found to be satisfactory. Figure 6 shows the temporal trend and seasonal component inferred for each model. The seasonal component is almost identical across all eight models. The temporal component is almost the same for the first six epidemic models, but differs evidently for the model without epidemics and the general-dependent model, with lower values in 2011-2013 and higher values in 2016-2019. Figure 7 shows the spatial component of the disease incidence risk, which looks very similar across the seven models with epidemics but different in the model without epidemics, especially for France, the Netherlands, Denmark, Norway and Sweden. These differences for the temporal and spatial components of the model without epidemics can be explained by the fact that under this model any increase in incidence caused by epidemics can only be explained by an increase in other model components. In the models with epidemics, the temporal, seasonal and spatial components look similar to a previous analysis of the untyped data [27], as would be expected given that these components affect all strains equally.

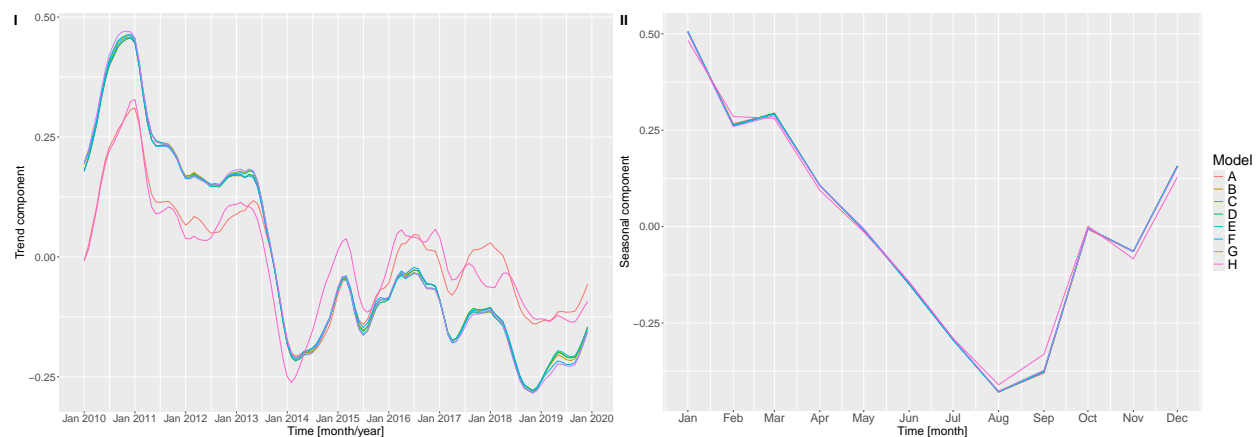


Figure 6: Posterior means for the meningococcal disease application of the trend components, and the seasonal components across all fitted models. (A) No epidemic model (B) Independent 1 model (C) Independent 2 model (D) Frank copula 1 model (F) Frank copula 2 model (G) Gaussian factor copula 1 model (H) Gaussian factor copula 2 model, and (H) General-dependent model.

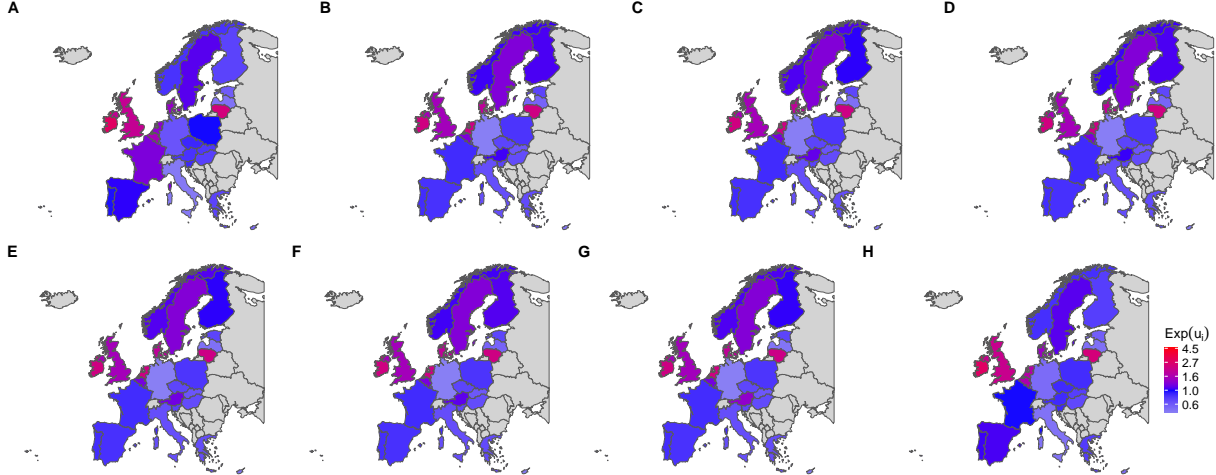


Figure 7: Posterior median relative risks (compared to the geometric mean risk, the mean of the log of the risk) for the meningococcal disease application from (A) No epidemic model (B) Independent 1 model (C) Independent 2 model (D) Frank copula 1 model (F) Frank copula 2 model (G) Gaussian factor copula 1 model (H) Gaussian factor copula 2 model, and (H) General-dependent model.

Figure 8 shows the inferred probabilities of the epidemic state in each country over time for each of the four types and for each of the seven epidemic models, with the notable exception of the general-dependent model which will be discussed later. These results are relatively consistent across models and show very clear dynamic differences between the four serogroups which could not have been investigated in an analysis of untyped data [27]. For the serogroup B countries typically stay in the endemic or epidemic state over many years, often spanning the whole study period. Serogroup W was endemic across all countries at the start of the study period in 2011, with the visually apparent exception of Cyprus and Luxembourg being caused by low populations and case numbers in these countries resulting in high uncertainty for all types and dates. Serogroup W switched to the epidemic state in several countries between 2013 and 2017, including Denmark, France, Ireland, Spain, Sweden and the UK, and for most of these countries stayed in the epidemic state until the end of 2019. Serogroups Y and C show a more mixed picture, with some countries such as France or Germany being in the epidemic state almost throughout and other countries switching between the two states several times during the study period, without much synchrony between countries. These results are in good agreement with a previous descriptive analysis of the evolution of invasive meningococcal disease in Europe [4]. In particular, this study noted the rise in serogroup W across several European countries with an overall increase of 517% from 2008 to 2017. Our analysis found that the UK was the first country to be affected in 2013, as previously noted [67, 68]. For serogroup Y, several countries (Belgium, Denmark, Finland, France, the Netherlands, Norway, Sweden and the UK) were reported to have notably higher incidences than other countries in 2017 [4] and our results show that these countries are in the epidemic state at that time.

Figure S3 shows the 95% posterior predictive credible intervals [69] for the number of cases for each strain. The real data are almost always contained in the 95% posterior predictive credible intervals across all models except the model without epidemics, particularly for serogroup W. Table 3 contains the log marginal likelihood for each model estimated by both the importance sampling [62] and bridge sampling [60] methods based on 50 repeated evaluations in an attempt to quantify the Monte Carlo standard error of our estimate. The two methods are in good agreement, both finding that model Frank copula 1 is most likely, with only the two Independent 1 and Gaussian copula 1 have non-negligible posterior probability. However, the importance sampling method gives a more balanced probability between these three models compared to the bridge sampling method. When the correlation parameters of the Frank copula 1 and Gaussian copula 1 models are small, they reduce to the Independent 1 model which explains why it is difficult here to distinguish between them. The three models with separate strain marginal distributions have lower posterior probabilities, indicating that there is no evidence against all strains having the same marginal behaviour. Finally, the general-dependent model had the lowest log marginal likelihood, indicating that the different results from this model (Figures 6 and 8) should not be trusted. This model can theoretically reduce to the same as the best models, but is handicapped by the large number of parameters in its transition matrix ($2^K(2^K - 1) = 240$ for $K = 4$).

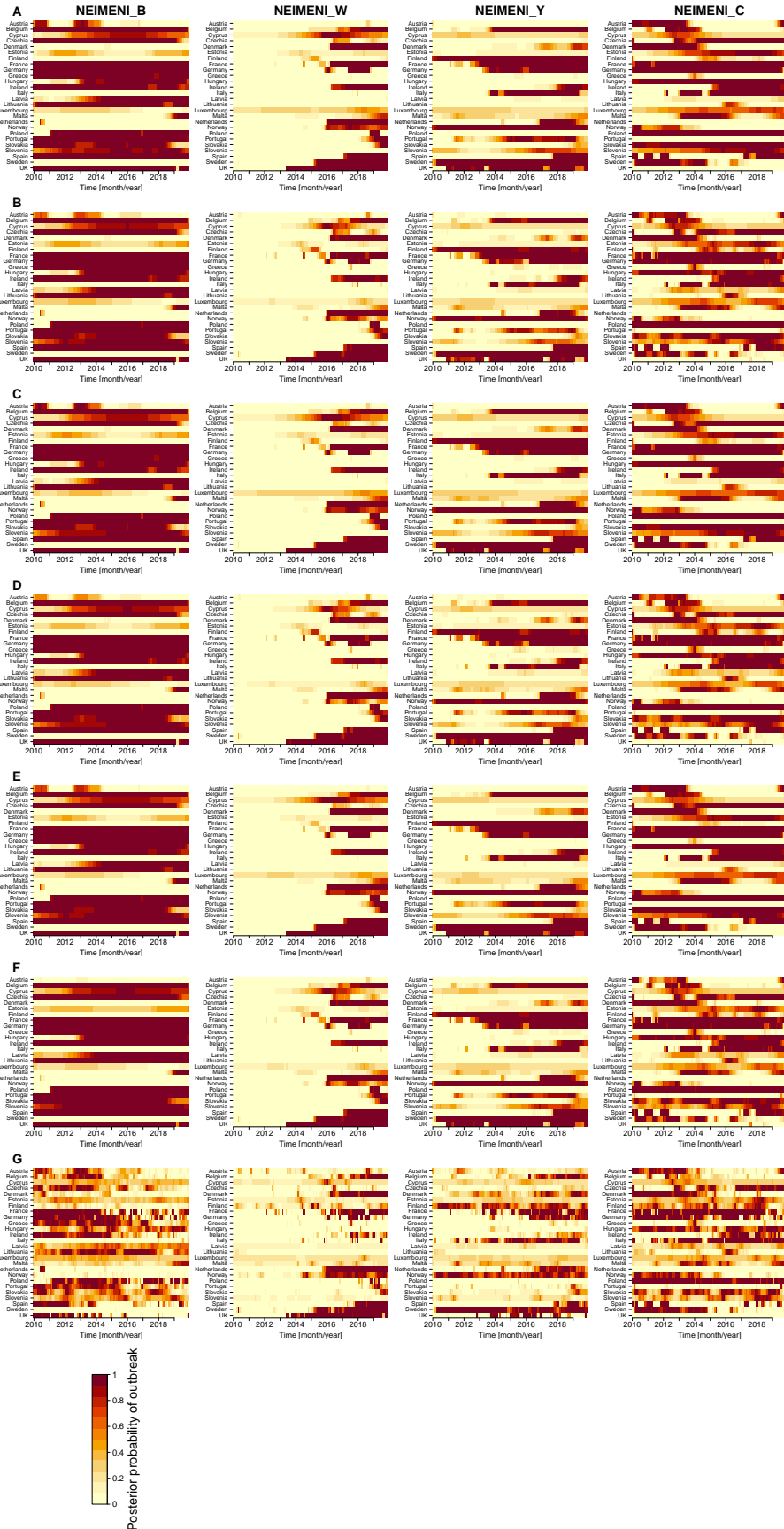


Figure 8: Heat-maps showing for the meningococcal disease application the posterior probability of the epidemic state using (A) Independent 1 model (B) Independent 2 model (C) Frank copula 1 model (D) Frank copula 2 model (E) Gaussian factor copula 1 model (F) Gaussian factor copula 2 model, and (G) General-dependent model.

Table 3: Model comparison for the multi-type meningococcal disease application with mean and standard deviations reported based on 50 repeated evaluations of the log marginal likelihood.

Model type	Log marginal likelihood		Posterior model probability	
	IS (SD)	BS (SD)	IS (SD)	BS (SD)
No epidemic	-17976.50 (1.03)	-18014.07 (0.17)	0.0000 (0.00)	0.0000 (0.00)
Independent 1	-15071.63 (0.96)	-15109.78 (0.16)	0.3079 (0.22)	0.0253 (0.00)
Independent 2	-15125.94 (1.48)	-15164.38 (0.19)	0.0000 (0.00)	0.0000 (0.00)
Frank copula 1	-15071.46 (1.20)	-15106.12 (0.23)	0.3911 (0.28)	0.9484 (0.01)
Frank copula 2	-15126.72 (1.50)	-15162.31 (0.18)	0.0000 (0.00)	0.0000 (0.00)
Gaussian factor copula 1	-15071.76 (1.39)	-15109.75 (0.20)	0.3009 (0.26)	0.0262 (0.00)
Gaussian factor copula 2	-15123.19 (1.81)	-15162.68 (0.25)	0.0000 (0.00)	0.0000 (0.00)
General-dependent	-18266.30 (22.29)	-15667.63 (2.15)	0.0000 (0.00)	0.0000 (0.00)

IS: importance sampling, BS: bridge sampling, SD: standard deviation.

5 Discussion

We have presented a new framework for the analysis of spatio-temporal epidemic data, which builds upon previous work [17, 26, 27] but has the key new feature of being able to handle multi-type data. We designed several models in which multiple types can cause epidemics with different dependency structures, exploiting probability theory on copulas [28]. For each model we showed how Bayesian inference can be performed, and also how Bayesian model comparison can reveal the most appropriate model for analysis.

As with any model design, the basic formulation in Equation 4 makes a number of assumptions that are worth discussing. In contrast to previous work [27], the models presented in this study incorporate strain-specific intercepts (a_k), which separates the intercept from the trend. This separation allows the intercepts to vary across strains while keeping the temporal components (r_t and s_t) fixed across strains. However, all strains share the same temporal components. Allowing each strain to have a separate temporal trend component (r_{tk}) would in principle be straightforward and potentially allow the estimation of interesting differences between strain dynamics. However, it would increase the number of parameters to estimate and they might suffer from identifiability issues vis-a-vis the epidemic terms (x_{itk}). We therefore did not attempt this extended parametrisation, although there might be some settings where it would be useful. Another potentially interesting avenue for future work would be to use a similar formulation to analyse multi-host data. This would be useful to study pathogens that can infect several species, for example *Salmonella enterica* or *Campylobacter jejuni*, but also to integrate relevant data on the host, for example the age of individuals infected with *Neisseria meningitidis* which is known to be associated with infection numbers in datasets such as the one we analysed here [4].

For the Bayesian inference we initially attempted to use the probabilistic programming software Stan [51]. It provides a versatile gradient-based MCMC sampler known as the No-U-Turn sampler (NUTS) which has contributed to the widespread accessibility of Bayesian computation to researchers from various disciplines. However, we found Stan to be inefficient with the models we proposed due to high dimensionality and the burden of computing the entire gradients of the log posterior in every leapfrog step via automatic differentiation. We therefore developed a bespoke MCMC sampling scheme using analytically derived gradients and observed Fisher information matrices to support efficient posterior exploration using a MMALA scheme [29]. This allowed us to analyse datasets at a scale and speed that would not have been possible otherwise.

To calculate the model evidences, we used both importance sampling [62] and bridge sampling [60]. Whilst the two methods were in agreement as to the best fitting model, we see a substantial disagreement in the overall level of the log marginal likelihood between the two methods that was much larger than the Monte Carlo standard errors. For the general-dependent model, the failure of the importance sampling method to produce comparable estimates probably stems from high-dimensionality of the posterior (for example, it has 240 transition parameters versus only 12 transition parameters in the Gaussian factor copula 2 model), and the fact that sampling the transmission probability vectors from a heavy-tail multivariate t distribution does not constrain them to lie within the 16 dimensional simplex, even when the mean vector satisfies this constraint. We attempted to solve the challenge by imposing a constraint to enforce the transition matrix to be a stochastic matrix, however, this only slightly improved the estimate and its associated Monte Carlo standard error. In contrast, the bridge sampling scheme performed well because it uses samples from both the posterior distribution and the proposal distribution within a well constructed bridge function whilst taking into account the required constraints of all model parameters, and therefore produces more reliable estimates.

In conclusion, the work presented here contains several innovations in the modelling of dependency between types of an infectious disease, in the Bayesian inference of parameters using Monte-Carlo techniques and in the model comparison methodology. Beyond our own goals, these methodological developments are likely to be useful to other scientific researchers developing methods to analyse large multi-factorial infectious disease datasets under complex parametric models. Furthermore, our inferential framework is implemented into an open source software which is generally applicable to a wide range of spatio-temporal epidemic data.

A Appendix

A.1 Temporal trend component

To estimate a smooth background temporal trend, the trend component, r_t , is assumed to follow a second-order Gaussian random walk prior given by

$$r_t | r_{t-1}, r_{t-2} = 2r_{t-1} - r_{t-2} + \epsilon_t,$$

for $t = 3, \dots, T$, where $\epsilon_t \sim \mathcal{N}(0, \kappa_r^{-1})$. The components of the temporal trend are forced to sum to zero, in contrast to the formulation in [27] where they also act as an intercept in the model.

The joint prior density of the trend components \mathbf{r} is written as

$$\mathbf{P}(\mathbf{r} | \kappa_r) \propto \kappa_r^{\frac{T-2}{2}} \exp\left(-\frac{\kappa_r}{2} \sum_{t=3}^T (r_t - 2r_{t-1} + r_{t-2})^2\right),$$

where κ_r is the precision parameter, with the constraint that $\sum_{t=1}^T r_t = 0$. An alternative formulation of this density is written as

$$\mathbf{P}(\mathbf{r} | \kappa_r) \propto \kappa_r^{\frac{T-2}{2}} \exp\left(-\frac{\kappa_r}{2} \mathbf{r}^\top \mathbf{R}_r \mathbf{r}\right) \mathbb{1}_{(\mathbf{r}^\top \mathbf{1}=0)} \quad (\text{A1})$$

where \mathbf{R}_r is a $T \times T$ structure matrix of the second-order Gaussian random walk (RW2) prior, describing the neighborhood structure of the components:

$$\mathbf{R}_r = \begin{bmatrix} 1 & -2 & 1 & 0 & 0 & 0 & \dots & 0 & 0 & 0 \\ -2 & 5 & -4 & 1 & 0 & 0 & \dots & 0 & 0 & 0 \\ 1 & -4 & 6 & -4 & 1 & 0 & \dots & 0 & 0 & 0 \\ 0 & 1 & -4 & 6 & -4 & 1 & \dots & 0 & 0 & 0 \\ \vdots & \vdots & \vdots & \vdots & \vdots & \vdots & \ddots & \vdots & \vdots & \vdots \\ 0 & 0 & 0 & 0 & 0 & 0 & \dots & 1 & -2 & 1 \end{bmatrix}$$

A.2 Seasonal component

We propose a first-order cyclic Gaussian random walk model for the seasonal components, s_t . This model is formulated such that the seasonal components are repeated throughout the time period, enabling the seasonal component to capture a static repeating pattern. The number of components in the cycle is chosen based on the structure of the available dataset and the epidemiology of the disease under study.

$$\mathbf{s} = (s_1, s_2, \dots, s_C),$$

$$s_c - s_{c-1} \sim \mathcal{N}(0, \kappa_s^{-1}),$$

$c = 2, \dots, C$ and $s_1 - s_C \sim \mathcal{N}(0, \kappa_s^{-1})$, so that s_1 and s_C are considered neighbouring components. The joint density for this prior is written as

$$\mathbf{P}(\mathbf{s} | \kappa_s) \propto (\kappa_s)^{\frac{C-1}{2}} \exp\left(-\frac{\kappa_s}{2} \mathbf{s}^\top \mathbf{R}_c \mathbf{s}\right) \mathbb{1}_{(\mathbf{s}^\top \mathbf{1}=0)} \quad (\text{A2})$$

where C represents the number of components in the cycle, and \mathbf{R}_c represents a $C \times C$ structure matrix for the cyclic first-order random walk model (cRW1). The resulting structure matrix is given by:

$$\mathbf{R}_c = \begin{bmatrix} 2 & -1 & 0 & 0 & 0 & 0 & \dots & -1 \\ -1 & 2 & -1 & 0 & 0 & 0 & \dots & 0 \\ 0 & -1 & 2 & -1 & 0 & 0 & \dots & 0 \\ 0 & 0 & -1 & 2 & -1 & 0 & \dots & 0 \\ \vdots & \vdots & \vdots & \vdots & \vdots & \vdots & \ddots & \vdots \\ -1 & 0 & 0 & 0 & 0 & 0 & \dots & -1 & 2 \end{bmatrix}$$

The sum-to-zero constraint, $\sum_{c=1}^C s_c = 0$, is imposed for identifiability of the seasonal components. We implement $C = 12$ for both the simulation and application. Thus, each component representing a month in a year and the cycle is forced to repeat over the entire period of the dataset.

A.3 Spatial component

For the spatial components, u_i , we assume a Gaussian intrinsic autoregression, also known as an intrinsic Gaussian Markov Random Field (IGMRF). This model is commonly used in disease mapping in the situation of low counts [70].

$$u_i|u_{-i} \sim \mathcal{N}\left(\sum_{j \in n(i)} \frac{u_j}{|n(i)|}, \frac{\sigma^2}{|n(i)|}\right),$$

where $n(i)$ is the set of indices of locations that neighbour location $i \in \{1, \dots, I\}$. The joint density of the spatial components \mathbf{u} is written as

$$\mathbb{P}(\mathbf{u}|\kappa_u) \propto \left(\frac{\kappa_u}{2\pi}\right)^{\frac{I-k}{2}} \exp\left(-\frac{\kappa_u}{2} \mathbf{u}^\top \mathbf{R}_u \mathbf{u}\right) \mathbb{1}_{(\mathbf{u}^\top \mathbf{1}=0)} \quad (\text{A3})$$

where \mathbf{R}_u is the structure matrix derived from a given adjacency matrix describing the connectivity of the geographical locations under study. \mathbf{R}_u has rank $I - k$, with k being its rank deficiency. The elements of \mathbf{R} are

$$R_{ij} = \begin{cases} |n(i)| & \text{if } i = j, \\ -1 & \text{if } j \in n(i), \\ 0 & \text{otherwise.} \end{cases}$$

Let \mathbf{Q} denote the precision matrix for an intrinsic Gaussian Markov random field, so that $\mathbf{Q}^{-1} = \mathbf{\Sigma}$ is its variance-covariance matrix. The matrix \mathbf{Q} is rank deficient due to the sum to zero constraint of the structure matrix, \mathbf{R}_u . This implies the non-invertibility of \mathbf{Q} , thus, $\mathbf{\Sigma}$ is undefined. Since IGMRFs are improper distributions, they cannot be generative models for data but can be used as priors for modelling [31]. Here, we derive the elements of the precision matrix for a first-order IGMRF for spatial components.

$$\text{Prec}(u_i) = Q_{ii} = \kappa_u |n(i)|$$

Assuming all spatial components have mean 0,

$$\begin{aligned} \mathbb{E}(u_i|u_{-i}) &= \sum_{j \in n(i)} \frac{u_j}{|n(i)|} = -\frac{1}{Q_{ii}} \sum_{j \in n(i)} Q_{ij} u_j \\ \Rightarrow Q_{ij} &= \begin{cases} -\kappa_u & j \in n(i) \\ \kappa_u |n(i)| & j = i \\ 0 & \text{otherwise.} \end{cases} \end{aligned}$$

Hence, $\mathbf{Q} = \kappa_u \times \mathbf{R}_u$.

A.4 Copula in the case with two strains

For $K = 2$, define u and v as the marginal probabilities that strains 1 and 2 transit to state 1 in the next step, respectively. The four joint probabilities are:

$$\begin{aligned} \mathbb{P}(0, 0) &= 1 - u - v + C(u, v) \\ \mathbb{P}(0, 1) &= v - C(u, v) \\ \mathbb{P}(1, 0) &= u - C(u, v) \\ \mathbb{P}(1, 1) &= C(u, v) \end{aligned}$$

The elements of the joint transition matrix are therefore:

From state $(0, 0)$, $u = p, v = p$

$$\begin{aligned} (0, 0) \rightarrow (0, 0) &= 1 - p - p + C(p, p) \\ (0, 0) \rightarrow (0, 1) &= p - C(p, p) \\ (0, 0) \rightarrow (1, 0) &= p - C(p, p) \\ (0, 0) \rightarrow (1, 1) &= C(p, p) \end{aligned}$$

From state $(0, 1)$, $u = p, v = 1 - q$

$$\begin{aligned} (0, 1) \rightarrow (0, 0) &= 1 - p - (1 - q) + C(p, 1 - q) \\ (0, 1) \rightarrow (0, 1) &= 1 - q - C(p, 1 - q) \\ (0, 1) \rightarrow (1, 0) &= p - C(p, 1 - q) \\ (0, 1) \rightarrow (1, 1) &= C(p, 1 - q) \end{aligned}$$

From state $(1, 0)$, $u = 1 - q, v = p$

$$\begin{aligned} (1, 0) \rightarrow (0, 0) &= 1 - (1 - q) - p + C(1 - q, p) \\ (1, 0) \rightarrow (0, 1) &= p - C(1 - q, p) \\ (1, 0) \rightarrow (1, 0) &= 1 - q - C(1 - q, p) \\ (1, 0) \rightarrow (1, 1) &= C(1 - q, p) \end{aligned}$$

From state $(1, 1)$, $u = 1 - q, v = 1 - q$

$$\begin{aligned} (1, 1) \rightarrow (0, 0) &= 1 - (1 - q) - (1 - q) + C(1 - q, 1 - q) \\ (1, 1) \rightarrow (0, 1) &= 1 - q - C(1 - q, 1 - q) \\ (1, 1) \rightarrow (1, 0) &= 1 - q - C(1 - q, 1 - q) \\ (1, 1) \rightarrow (1, 1) &= C(1 - q, 1 - q) \end{aligned}$$

A.5 Copula in the case with three strains

For $K = 3$, define u , v and w as the marginal probabilities that strains 1, 2 and 3 transit to state 1 in the next step, respectively. The eight joint probabilities are given by the standard inclusion-exclusion representation of the joint cumulative distribution function of a 3-dimensional copula:

$$\begin{aligned} \mathbb{P}(0, 0, 0) &= 1 - u - v - w + C(u, v, 1) + C(u, 1, w) + C(1, v, w) - C(u, v, w) \\ \mathbb{P}(0, 0, 1) &= w - C(u, 1, w) - C(1, v, w) + C(u, v, w) \\ \mathbb{P}(0, 1, 0) &= v - C(u, v, 1) - C(1, v, w) + C(u, v, w) \\ \mathbb{P}(1, 0, 0) &= u - C(u, v, 1) - C(u, 1, w) + C(u, v, w) \\ \mathbb{P}(0, 1, 1) &= C(1, v, w) - C(u, v, w) \\ \mathbb{P}(1, 0, 1) &= C(u, 1, w) - C(u, v, w) \\ \mathbb{P}(1, 1, 0) &= C(u, v, 1) - C(u, v, w) \\ \mathbb{P}(1, 1, 1) &= C(u, v, w) \end{aligned}$$

The elements of the joint transition matrix are:

From state $(0, 0, 0)$, $u = p, v = p, w = p$

$$\begin{aligned} (0, 0, 0) \rightarrow (0, 0, 0) &= 1 - p - p - p + C(p, p, 1) + C(p, 1, p) + C(1, p, p) - C(p, p, p) \\ (0, 0, 0) \rightarrow (0, 0, 1) &= p - C(p, 1, p) - C(1, p, p) + C(p, p, p) \\ (0, 0, 0) \rightarrow (0, 1, 0) &= p - C(p, p, 1) - C(1, p, p) + C(p, p, p) \\ (0, 0, 0) \rightarrow (1, 0, 0) &= p - C(p, p, 1) - C(p, 1, p) + C(p, p, p) \\ (0, 0, 0) \rightarrow (0, 1, 1) &= C(1, p, p) - C(p, p, p) \\ (0, 0, 0) \rightarrow (1, 0, 1) &= C(p, 1, p) - C(p, p, p) \\ (0, 0, 0) \rightarrow (1, 1, 0) &= C(p, p, 1) - C(p, p, p) \\ (0, 0, 0) \rightarrow (1, 1, 1) &= C(p, p, p) \end{aligned}$$

From state $(0, 0, 1)$, $u = p, v = p, w = 1 - q$

$$\begin{aligned} (0, 0, 1) \rightarrow (0, 0, 0) &= 1 - p - p - (1 - q) + C(p, p, 1) + C(p, 1, 1 - q) + C(1, p, 1 - q) - C(p, p, 1 - q) \\ (0, 0, 1) \rightarrow (0, 0, 1) &= (1 - q) - C(p, 1, 1 - q) - C(1, p, 1 - q) + C(p, p, 1 - q) \\ (0, 0, 1) \rightarrow (0, 1, 0) &= p - C(p, p, 1) - C(1, p, 1 - q) + C(p, p, 1 - q) \\ (0, 0, 1) \rightarrow (1, 0, 0) &= p - C(p, p, 1) - C(p, 1, 1 - q) + C(p, p, 1 - q) \\ (0, 0, 1) \rightarrow (0, 1, 1) &= C(1, p, 1 - q) - C(p, p, 1 - q) \\ (0, 0, 1) \rightarrow (1, 0, 1) &= C(p, 1, 1 - q) - C(p, p, 1 - q) \\ (0, 0, 1) \rightarrow (1, 1, 0) &= C(p, p, 1) - C(p, p, 1 - q) \\ (0, 0, 1) \rightarrow (1, 1, 1) &= C(p, p, 1 - q) \end{aligned}$$

From state $(0, 1, 0)$, $u = p, v = 1 - q, w = p$

$$\begin{aligned} (0, 1, 0) \rightarrow (0, 0, 0) &= 1 - p - (1 - q) - p + C(p, 1 - q, 1) + C(p, 1, p) + C(1, 1 - q, p) - C(p, 1 - q, p) \\ (0, 1, 0) \rightarrow (0, 0, 1) &= p - C(p, 1, p) - C(1, 1 - q, p) + C(p, 1 - q, p) \\ (0, 1, 0) \rightarrow (0, 1, 0) &= (1 - q) - C(p, 1 - q, 1) - C(1, 1 - q, p) + C(p, 1 - q, p) \\ (0, 1, 0) \rightarrow (1, 0, 0) &= p - C(p, 1 - q, 1) - C(p, 1, p) + C(p, 1 - q, p) \\ (0, 1, 0) \rightarrow (0, 1, 1) &= C(1, 1 - q, p) - C(p, 1 - q, p) \\ (0, 1, 0) \rightarrow (1, 0, 1) &= C(p, 1, p) - C(p, 1 - q, p) \\ (0, 1, 0) \rightarrow (1, 1, 0) &= C(p, 1 - q, 1) - C(p, 1 - q, p) \\ (0, 1, 0) \rightarrow (1, 1, 1) &= C(p, 1 - q, p) \end{aligned}$$

From state $(1, 0, 0)$, $u = 1 - q, v = p, w = p$

$$\begin{aligned} (1, 0, 0) \rightarrow (0, 0, 0) &= 1 - (1 - q) - p - p + C(1 - q, p, 1) + C(1 - q, 1, p) + C(p, p, 1) - C(1 - q, p, p) \\ (1, 0, 0) \rightarrow (0, 0, 1) &= p - C(1 - q, 1, p) - C(p, p, 1) + C(1 - q, p, p) \\ (1, 0, 0) \rightarrow (0, 1, 0) &= p - C(1 - q, p, 1) - C(p, p, 1) + C(1 - q, p, p) \\ (1, 0, 0) \rightarrow (1, 0, 0) &= (1 - q) - C(1 - q, p, 1) - C(1 - q, 1, p) + C(1 - q, p, p) \\ (1, 0, 0) \rightarrow (0, 1, 1) &= C(p, p, 1) - C(1 - q, p, p) \\ (1, 0, 0) \rightarrow (1, 0, 1) &= C(1 - q, 1, p) - C(1 - q, p, p) \\ (1, 0, 0) \rightarrow (1, 1, 0) &= C(1 - q, p, 1) - C(1 - q, p, p) \\ (1, 0, 0) \rightarrow (1, 1, 1) &= C(1 - q, p, p) \end{aligned}$$

From state $(0, 1, 1)$, $u = p, v = 1 - q, w = 1 - q$

$$\begin{aligned} (0, 1, 1) \rightarrow (0, 0, 0) &= 1 - p - (1 - q) - (1 - q) + C(p, 1 - q, 1) + C(p, 1, 1 - q) + C(1, 1 - q, 1 - q) - C(p, 1 - q, 1 - q) \\ (0, 1, 1) \rightarrow (0, 0, 1) &= (1 - q) - C(p, 1, 1 - q) - C(1, 1 - q, 1 - q) + C(p, 1 - q, 1 - q) \\ (0, 1, 1) \rightarrow (0, 1, 0) &= (1 - q) - C(p, 1 - q, 1) - C(1, 1 - q, 1 - q) + C(p, 1 - q, 1 - q) \\ (0, 1, 1) \rightarrow (1, 0, 0) &= p - C(p, 1 - q, 1) - C(p, 1, 1 - q) + C(p, 1 - q, 1 - q) \\ (0, 1, 1) \rightarrow (0, 1, 1) &= C(1, 1 - q, 1 - q) - C(p, 1 - q, 1 - q) \\ (0, 1, 1) \rightarrow (1, 0, 1) &= C(p, 1, 1 - q) - C(p, 1 - q, 1 - q) \\ (0, 1, 1) \rightarrow (1, 1, 0) &= C(p, 1 - q, 1) - C(p, 1 - q, 1 - q) \\ (0, 1, 1) \rightarrow (1, 1, 1) &= C(p, 1 - q, 1 - q) \end{aligned}$$

From state $(1, 0, 1)$, $u = 1 - q, v = p, w = 1 - q$

$$(1, 0, 1) \rightarrow (0, 0, 0) = 1 - (1 - q) - p - (1 - q) + C(1 - q, p, 1) + C(1 - q, 1, 1 - q) + C(p, 1, 1 - q) - C(1 - q, p, 1 - q)$$

$$(1, 0, 1) \rightarrow (0, 0, 1) = (1 - q) - C(1 - q, 1, 1 - q) - C(p, 1, 1 - q) + C(1 - q, p, 1 - q)$$

$$(1, 0, 1) \rightarrow (0, 1, 0) = p - C(1 - q, p, 1) - C(p, 1, 1 - q) + C(1 - q, p, 1 - q)$$

$$(1, 0, 1) \rightarrow (1, 0, 0) = (1 - q) - C(1 - q, p, 1) - C(1 - q, 1, 1 - q) + C(1 - q, p, 1 - q)$$

$$(1, 0, 1) \rightarrow (0, 1, 1) = C(p, 1, 1 - q) - C(1 - q, p, 1 - q)$$

$$(1, 0, 1) \rightarrow (1, 0, 1) = C(1 - q, 1, 1 - q) - C(1 - q, p, 1 - q)$$

$$(1, 0, 1) \rightarrow (1, 1, 0) = C(1 - q, p, 1) - C(1 - q, p, 1 - q)$$

$$(1, 0, 1) \rightarrow (1, 1, 1) = C(1 - q, p, 1 - q)$$

From state $(1, 1, 0)$, $u = 1 - q, v = 1 - q, w = p$

$$(1, 1, 0) \rightarrow (0, 0, 0) = 1 - (1 - q) - (1 - q) - p + C(1 - q, 1 - q, 1) + C(1 - q, 1, p) + C(1 - q, p, 1) - C(1 - q, 1 - q, p)$$

$$(1, 1, 0) \rightarrow (0, 0, 1) = p - C(1 - q, 1, p) - C(1 - q, p, 1) + C(1 - q, 1 - q, p)$$

$$(1, 1, 0) \rightarrow (0, 1, 0) = (1 - q) - C(1 - q, 1 - q, 1) - C(1 - q, 1, p) + C(1 - q, 1 - q, p)$$

$$(1, 1, 0) \rightarrow (1, 0, 0) = (1 - q) - C(1 - q, 1 - q, 1) - C(1 - q, p, 1) + C(1 - q, 1 - q, p)$$

$$(1, 1, 0) \rightarrow (0, 1, 1) = C(1 - q, p, 1) - C(1 - q, 1 - q, p)$$

$$(1, 1, 0) \rightarrow (1, 0, 1) = C(1 - q, 1, p) - C(1 - q, 1 - q, p)$$

$$(1, 1, 0) \rightarrow (1, 1, 0) = C(1 - q, 1 - q, 1) - C(1 - q, 1 - q, p)$$

$$(1, 1, 0) \rightarrow (1, 1, 1) = C(1 - q, 1 - q, p)$$

From state $(1, 1, 1)$, $u = 1 - q, v = 1 - q, w = 1 - q$

$$(1, 1, 1) \rightarrow (0, 0, 0) = 1 - (1 - q) - (1 - q) - (1 - q) + C(1 - q, 1 - q, 1) + C(1 - q, 1, 1 - q) + C(1, 1 - q, 1 - q) - C(1 - q, 1 - q, 1 - q)$$

$$(1, 1, 1) \rightarrow (0, 0, 1) = (1 - q) - C(1 - q, 1, 1 - q) - C(1 - q, 1 - q, 1) + C(1 - q, 1 - q, 1 - q)$$

$$(1, 1, 1) \rightarrow (0, 1, 0) = (1 - q) - C(1 - q, 1 - q, 1) - C(1 - q, 1, 1 - q) + C(1 - q, 1 - q, 1 - q)$$

$$(1, 1, 1) \rightarrow (1, 0, 0) = (1 - q) - C(1 - q, 1 - q, 1) - C(1 - q, 1, 1 - q) + C(1 - q, 1 - q, 1 - q)$$

$$(1, 1, 1) \rightarrow (0, 1, 1) = C(1 - q, 1 - q, 1) - C(1 - q, 1 - q, 1 - q)$$

$$(1, 1, 1) \rightarrow (1, 0, 1) = C(1 - q, 1, 1 - q) - C(1 - q, 1 - q, 1 - q)$$

$$(1, 1, 1) \rightarrow (1, 1, 0) = C(1 - q, 1 - q, 1) - C(1 - q, 1 - q, 1 - q)$$

$$(1, 1, 1) \rightarrow (1, 1, 1) = C(1 - q, 1 - q, 1 - q).$$

A.6 Gradients and Hessians from the log likelihood and log priors

The gradients and Hessians from the log likelihood with respect to \mathbf{r} , \mathbf{s} and \mathbf{u} are:

$$\begin{aligned}\nabla_{\mathbf{r}} \log \mathbb{P}(\mathbf{y}_{1:I,1:T,1:K}|\boldsymbol{\theta}) &= \left[\sum_{i=1}^I \sum_{k=1}^K (y_{i1k} - \eta_{i1k}), \dots, \sum_{i=1}^I \sum_{k=1}^K (y_{iT k} - \eta_{iT k}) \right]^{\top} \\ \nabla_{\mathbf{r}}^2 \log \mathbb{P}(\mathbf{y}_{1:I,1:T,1:K}|\boldsymbol{\theta}) &\approx \text{diag} \left[\sum_{i=1}^I \sum_{k=1}^K (-\eta_{i1k}), \dots, \sum_{i=1}^I \sum_{k=1}^K (-\eta_{iT k}) \right] \\ \nabla_{\mathbf{s}} \log \mathbb{P}(\mathbf{y}_{1:I,1:T,1:K}|\boldsymbol{\theta}) &= \left[\sum_{t:t \bmod C=1} \sum_{i=1}^I \sum_{k=1}^K (y_{itk} - \eta_{itk}), \dots, \sum_{t:t \bmod C=C} \sum_{i=1}^I \sum_{k=1}^K (y_{itk} - \eta_{itk}) \right]^{\top} \\ \nabla_{\mathbf{s}}^2 \log \mathbb{P}(\mathbf{y}_{1:I,1:T,1:K}|\boldsymbol{\theta}) &\approx \text{diag} \left[\sum_{t:t \bmod C=1} \sum_{i=1}^I \sum_{k=1}^K (-\eta_{itk}), \dots, \sum_{t:t \bmod C=C} \sum_{i=1}^I \sum_{k=1}^K (-\eta_{itk}) \right] \\ \nabla_{\mathbf{u}} \log \mathbb{P}(\mathbf{y}_{1:I,1:T,1:K}|\boldsymbol{\theta}) &= \left[\sum_{t=1}^T \sum_{k=1}^K (y_{1tk} - \eta_{1tk}), \dots, \sum_{t=1}^T \sum_{k=1}^K (y_{Itk} - \eta_{Itk}) \right]^{\top} \\ \nabla_{\mathbf{u}}^2 \log \mathbb{P}(\mathbf{y}_{1:I,1:T,1:K}|\boldsymbol{\theta}) &\approx \text{diag} \left[\sum_{t=1}^T \sum_{k=1}^K (-\eta_{1tk}), \dots, \sum_{t=1}^T \sum_{k=1}^K (-\eta_{Itk}) \right]\end{aligned}$$

The log prior densities for the temporal and spatial components are given by:

$$\begin{aligned}\log \mathbb{P}(\mathbf{r}|\kappa_r) &= -\frac{\kappa_r}{2} \mathbf{r}^{\top} \mathbf{R}_r \mathbf{r} + \text{Const} \\ \log \mathbb{P}(\mathbf{s}|\kappa_s) &= -\frac{\kappa_s}{2} \mathbf{s}^{\top} \mathbf{R}_c \mathbf{s} + \text{Const} \\ \log \mathbb{P}(\mathbf{u}|\kappa_u) &= -\frac{\kappa_u}{2} \mathbf{u}^{\top} \mathbf{R}_u \mathbf{u} + \text{Const}\end{aligned}$$

The gradients and Hessians for these log prior densities with respect to \mathbf{r} , \mathbf{s} and \mathbf{u} are:

$$\begin{aligned}\nabla_{\mathbf{r}} \log \mathbb{P}(\mathbf{r}|\kappa_r) &= \frac{-\kappa_r(\mathbf{R}_r + \mathbf{R}_r^{\top})\mathbf{r}}{2} = -\kappa_r \mathbf{R}_r \mathbf{r} \\ \nabla_{\mathbf{s}} \log \mathbb{P}(\mathbf{s}|\kappa_s) &= \frac{-\kappa_s(\mathbf{R}_c + \mathbf{R}_c^{\top})\mathbf{s}}{2} = -\kappa_s \mathbf{R}_c \mathbf{s} \\ \nabla_{\mathbf{u}} \log \mathbb{P}(\mathbf{u}|\kappa_u) &= \frac{-\kappa_u(\mathbf{R}_u + \mathbf{R}_u^{\top})\mathbf{u}}{2} = -\kappa_u \mathbf{R}_u \mathbf{u} \\ \nabla_{\mathbf{r}}^2 \log \mathbb{P}(\mathbf{r}|\kappa_r) &= -\kappa_r \mathbf{R}_r \\ \nabla_{\mathbf{s}}^2 \log \mathbb{P}(\mathbf{s}|\kappa_s) &= -\kappa_s \mathbf{R}_c \\ \nabla_{\mathbf{u}}^2 \log \mathbb{P}(\mathbf{u}|\kappa_u) &= -\kappa_u \mathbf{R}_u\end{aligned}$$

References

- [1] Fred Neufeld. Ueber die agglutination der pneumokokken und über die theorieen der agglutination. *Zeitschrift für Hygiene und Infektionskrankheiten*, 40(1):54–72, 1902.
- [2] Ana Rita Narciso, Rebecca Dookie, Priyanka Nannapaneni, Staffan Normark, and Birgitta Henriques-Normark. Streptococcus pneumoniae epidemiology, pathogenesis and control. *Nature Reviews Microbiology*, 23(4):256–271, 2025.
- [3] Nadine G Roupheal and David S Stephens. Neisseria meningitidis: biology, microbiology, and epidemiology. *Neisseria meningitidis: advanced methods and protocols*, pages 1–20, 2011.
- [4] Charles Nuttens, Jamie Findlow, Paul Balmer, David L Swerdlow, and Myint Tin Tin Htar. Evolution of invasive meningococcal disease epidemiology in Europe, 2008 to 2017. *Eurosurveillance*, 27(3):2002075, 2022.
- [5] Syed M Jamal and Graham J Belsham. Foot-and-mouth disease: past, present and future. *Veterinary research*, 44(1):116, 2013.
- [6] Martin CJ Maiden. Multilocus sequence typing of bacteria. *Annu. Rev. Microbiol.*, 60(1):561–588, 2006.
- [7] Ian M Mackay, Katherine E Arden, and Andreas Nitsche. Real-time PCR in virology. *Nucleic acids research*, 30(6):1292–1305, 2002.
- [8] Stephen A Bustin and Reinhold Mueller. Real-time reverse transcription PCR (qRT-PCR) and its potential use in clinical diagnosis. *Clinical Science*, 109(4):365–379, 2005.
- [9] Fred Brauer. Compartmental models in epidemiology. In *Mathematical epidemiology*, pages 19–79. Springer, 2008.
- [10] William Ogilvy Kermack and Anderson G McKendrick. A contribution to the mathematical theory of epidemics. *Proceedings of the Royal Society of London. Series A, Containing papers of a mathematical and physical character*, 115(772):700–721, 1927.
- [11] Julia R Gog and Bryan T Grenfell. Dynamics and selection of many-strain pathogens. *Proceedings of the National Academy of Sciences*, 99(26):17209–17214, 2002.
- [12] C. Castillo-Chavez, H. W. Hethcote, V. Andreasen, S. A. Levin, and W. M. Liu. Epidemiological models with age structure, proportionate mixing, and cross-immunity. *Journal of Mathematical Biology*, 27(3):233–258, May 1989.
- [13] LJ White, MJ Cox, and GF Medley. Cross immunity and vaccination against multiple microparasite strains. *Mathematical Medicine and Biology: A Journal of the IMA*, 15(3):211–233, 1998.
- [14] Olivier Restif and Bryan T Grenfell. Integrating life history and cross-immunity into the evolutionary dynamics of pathogens. *Proceedings of the Royal Society B: Biological Sciences*, 273(1585):409–416, February 2006.
- [15] Ted Cohen, Marc Lipsitch, Rochelle P Walensky, and Megan Murray. Beneficial and perverse effects of isoniazid preventive therapy for latent tuberculosis infection in HIV–tuberculosis coinfecting populations. *Proceedings of the National Academy of Sciences*, 103(18):7042–7047, 2006.
- [16] Ian H Spicknall, Betsy Foxman, Carl F Marrs, and Joseph NS Eisenberg. A modeling framework for the evolution and spread of antibiotic resistance: literature review and model categorization. *American Journal of Epidemiology*, 178(4):508–520, 2013.
- [17] Leonhard Knorr-Held and Sylvia Richardson. A hierarchical model for space–time surveillance data on meningococcal disease incidence. *Journal of the Royal Statistical Society Series C: Applied Statistics*, 52(2):169–183, 2003.
- [18] Khandoker Shuvo Bakar and Sujit K Sahu. spTimer: Spatio-temporal Bayesian modeling using R. *Journal of Statistical Software*, 63:1–32, 2015.
- [19] Sebastian Meyer, Leonhard Held, and Michael Höhle. Spatio-temporal analysis of epidemic phenomena using the R package surveillance. *Journal of Statistical Software*, 77:1–55, 2017.
- [20] Neil M Ferguson, Derek AT Cummings, Simon Cauchemez, Christophe Fraser, Steven Riley, Aronrag Meeyai, Sophon Iamsirithaworn, and Donald S Burke. Strategies for containing an emerging influenza pandemic in Southeast Asia. *Nature*, 437(7056):209–214, 2005.
- [21] Håkan Andersson and Tom Britton. *Stochastic epidemic models and their statistical analysis*, volume 151. Springer Science & Business Media, 2012.
- [22] Stephanie M Fingerhuth, Sebastian Bonhoeffer, Nicola Low, and Christian L Althaus. Antibiotic-resistant Neisseria gonorrhoeae spread faster with more treatment, not more sexual partners. *PLoS pathogens*, 12(5):e1005611, 2016.

- [23] Lilith K Whittles, Peter J White, and Xavier Didelot. Estimating the fitness cost and benefit of cefixime resistance in *Neisseria gonorrhoeae* to inform prescription policy: a modelling study. *PLoS medicine*, 14(10):e1002416, 2017.
- [24] Patrick GT Walker, Charles Whittaker, Oliver J Watson, Marc Baguelin, Peter Winskill, Arran Hamlet, Bimandra A Djafaara, Zulma Cucunubá, Daniela Olivera Mesa, Will Green, et al. The impact of COVID-19 and strategies for mitigation and suppression in low-and middle-income countries. *Science*, 369(6502):413–422, 2020.
- [25] Louise Dyson, Edward M Hill, Sam Moore, Jacob Curran-Sebastian, Michael J Tildesley, Katrina A Lythgoe, Thomas House, Lorenzo Pellis, and Matt J Keeling. Possible future waves of SARS-CoV-2 infection generated by variants of concern with a range of characteristics. *Nature communications*, 12(1):5730, 2021.
- [26] Simon EF Spencer, Jonathan Marshall, Ruth Pirie, Donald Campbell, and Nigel P French. The detection of spatially localised outbreaks in campylobacteriosis notification data. *Spatial and spatio-temporal epidemiology*, 2(3):173–183, 2011.
- [27] Matthew Adeoye, Xavier Didelot, and Simon E.F. Spencer. Bayesian spatio-temporal modelling for infectious disease outbreak detection. *Epidemics*, 54:100879, 2026.
- [28] Roger B Nelsen. *An introduction to copulas*. Springer, 2006.
- [29] Mark Girolami and Ben Calderhead. Riemann manifold Langevin and Hamiltonian Monte Carlo methods. *Journal of the Royal Statistical Society Series B: Statistical Methodology*, 73(2):123–214, 2011.
- [30] European Centre for Disease Prevention and Control (ECDC). ECDC ATLAS Database, 2024. Accessed: 2024-10-30.
- [31] Havard Rue and Leonhard Held. *Gaussian Markov random fields: theory and applications*. Chapman and Hall/CRC, 2005.
- [32] M Sklar. Fonctions de répartition à n dimensions et leurs marges. In *Annales de l'ISUP*, volume 8, pages 229–231, 1959.
- [33] Marius Hofert, Ivan Kojadinovic, Martin Mächler, and Jun Yan. *Elements of copula modeling with R*. Springer, 2018.
- [34] Harry Joe. *Dependence modeling with copulas*. CRC press, 2014.
- [35] Pavel Krupskii and Harry Joe. Factor copula models for multivariate data. *Journal of Multivariate Analysis*, 120:85–101, 2013.
- [36] Walter Zucchini and Iain L MacDonald. *Hidden Markov models for time series: an introduction using R*. Chapman and Hall/CRC, 2009.
- [37] Hung-Wen Yeh, Wenyaw Chan, and Elaine Symanski. Intermittent missing observations in discrete-time hidden Markov models. *Communications in Statistics-Simulation and Computation*, 41(2):167–181, 2012.
- [38] Jackie Benschop, Shahista Nisa, and Simon EF Spencer. Still ‘dairy farm fever’? A Bayesian model for leptospirosis notification data in New Zealand. *Journal of the Royal Society Interface*, 18(175), 2021.
- [39] Valen E Johnson and David Rossell. On the use of non-local prior densities in Bayesian hypothesis tests. *Journal of the Royal Statistical Society Series B: Statistical Methodology*, 72(2):143–170, 2010.
- [40] Simon Duane, Anthony D Kennedy, Brian J Pendleton, and Duncan Roweth. Hybrid Monte Carlo. *Physics letters B*, 195(2):216–222, 1987.
- [41] Radford M Neal et al. MCMC using Hamiltonian dynamics. *Handbook of markov chain monte carlo*, 2(11):2, 2011.
- [42] Gareth O Roberts and Richard L Tweedie. Exponential convergence of Langevin distributions and their discrete approximations. *Bernoulli*, 2:341–363, 1996.
- [43] Gareth O Roberts and Jeffrey S Rosenthal. Optimal scaling of discrete approximations to Langevin diffusions. *Journal of the Royal Statistical Society: Series B (Statistical Methodology)*, 60(1):255–268, 1998.
- [44] Nicholas Metropolis, Arianna W Rosenbluth, Marshall N Rosenbluth, Augusta H Teller, and Edward Teller. Equation of state calculations by fast computing machines. *The journal of chemical physics*, 21(6):1087–1092, 1953.
- [45] W Keith Hastings. Monte Carlo sampling methods using Markov chains and their applications. *Biometrika*, 57:97–109, 1970.
- [46] Edgar C Merkle, Ellen Fitzsimmons, James Uanhoro, and Ben Goodrich. Efficient Bayesian structural equation modeling in Stan. *Journal of Statistical Software*, 100:1–22, 2021.

- [47] Herbert Robbins and Sutton Monro. A stochastic approximation method. *The annals of mathematical statistics*, pages 400–407, 1951.
- [48] Simon EF Spencer, Oliver Laeyendecker, Louise Dyson, Yu-Hsiang Hsieh, Eshan U Patel, Richard E Rothman, Gabor D Kelen, Thomas C Quinn, and T Deirdre Hollingsworth. Estimating HIV, HCV and HSV2 incidence from emergency department serosurvey. *Gates Open Research*, 5(116):116, 2021.
- [49] Matti Vihola. On the stability and ergodicity of adaptive scaling Metropolis algorithms. *Stochastic processes and their applications*, 121(12):2839–2860, 2011.
- [50] Simon EF Spencer. Accelerating adaptation in the adaptive Metropolis–Hastings random walk algorithm. *Australian & New Zealand Journal of Statistics*, 63(3):468–484, 2021.
- [51] Bob Carpenter, Andrew Gelman, Matthew D Hoffman, Daniel Lee, Ben Goodrich, Michael Betancourt, Marcus A Brubaker, Jiqiang Guo, Peter Li, and Allen Riddell. Stan: A probabilistic programming language. *Journal of statistical software*, 76, 2017.
- [52] Feng Qin, Anthony Auerbach, and Frederick Sachs. A direct optimization approach to hidden Markov modeling for single channel kinetics. *Biophysical journal*, 79(4):1915–1927, 2000.
- [53] Theodore C Lystig and James P Hughes. Exact computation of the observed information matrix for hidden Markov models. *Journal of Computational and Graphical Statistics*, 11(3):678–689, 2002.
- [54] Rolf Turner. Direct maximization of the likelihood of a hidden Markov model. *Computational Statistics & Data Analysis*, 52(9):4147–4160, 2008.
- [55] Thomas A Louis. Finding the observed information matrix when using the EM algorithm. *Journal of the Royal Statistical Society Series B: Statistical Methodology*, 44(2):226–233, 1982.
- [56] Randal Douc, Eric Moulines, and David Stoffer. *Nonlinear time series: Theory, methods and applications with R examples*. CRC press, 2014.
- [57] Emilio Zappa, Miranda Holmes-Cerfon, and Jonathan Goodman. Monte Carlo on manifolds: sampling densities and integrating functions. *Communications on Pure and Applied Mathematics*, 71(12):2609–2647, 2018.
- [58] Robert E Kass and Adrian E Raftery. Bayes factors. *Journal of the American Statistical Association*, 90(430):773–795, 1995.
- [59] Harold Jeffreys. *The theory of probability*. OuP Oxford, 1998.
- [60] Quentin F Gronau, Alexandra Sarafoglou, Dora Matzke, Alexander Ly, Udo Boehm, Maarten Marsman, David S Leslie, Jonathan J Forster, Eric-Jan Wagenmakers, and Helen Steingroever. A tutorial on bridge sampling. *Journal of Mathematical Psychology*, 81:80–97, 2017.
- [61] Antony M Overstall and Jonathan J Forster. Default Bayesian model determination methods for generalised linear mixed models. *Computational Statistics & Data Analysis*, 54(12):3269–3288, 2010.
- [62] Panayiota Touloupou, Naif Alzahrani, Peter Neal, Simon E. F. Spencer, and Trevelyan J. McKinley. Efficient model comparison techniques for models requiring large scale data augmentation. *Bayesian Analysis*, 13(2):437 – 459, 2018.
- [63] Quentin F. Gronau, Henrik Singmann, and Eric-Jan Wagenmakers. bridgesampling: An R package for estimating normalizing constants. *Journal of Statistical Software*, 92(10):1–29, 2020.
- [64] Eurostat. Eurostat Database, 2024. Accessed: 2024-11-05.
- [65] K Gleditsch and NB Weidmann. Mapping and measuring country shapes: The CShapes package. *R J*, 2:18–23, 2010.
- [66] Martyn Plummer, Nicky Best, Kate Cowles, Karen Vines, et al. CODA: convergence diagnosis and output analysis for MCMC. *R news*, 6(1):7–11, 2006.
- [67] Shamez N Ladhani, Kazim Beebeejaun, Jay Lucidarme, Helen Campbell, Steve Gray, Ed Kaczmarek, Mary E Ramsay, and Ray Borrow. Increase in endemic Neisseria meningitidis capsular group W sequence type 11 complex associated with severe invasive disease in England and Wales. *Clinical Infectious Diseases*, 60(4):578–585, 2015.
- [68] Manuel Krone, Steve Gray, Raquel Abad, Anna Skoczyńska, Paola Stefanelli, Arie van der Ende, Georgina Tzanakaki, Paula Mölling, Maria João Simões, Pavla Křížová, et al. Increase of invasive meningococcal serogroup W disease in Europe, 2013 to 2017. *Eurosurveillance*, 24(14):1800245, 2019.
- [69] Andrew Gelman, Xiao-Li Meng, and Hal Stern. Posterior predictive assessment of model fitness via realized discrepancies. *Statistica sinica*, pages 733–760, 1996.
- [70] Julian Besag, Jeremy York, and Annie Mollié. Bayesian image restoration, with two applications in spatial statistics. *Annals of the institute of statistical mathematics*, 43:1–20, 1991.

Supplementary Material

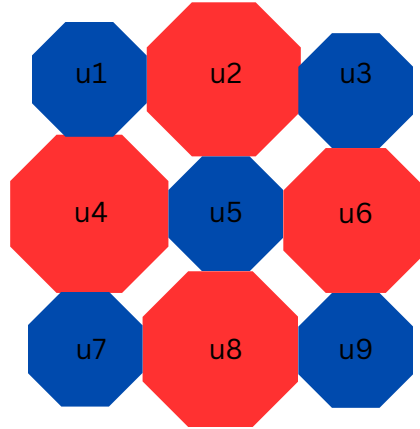


Figure S1: Adjacency structure of spatial locations with small cities in blue and large cities in red.

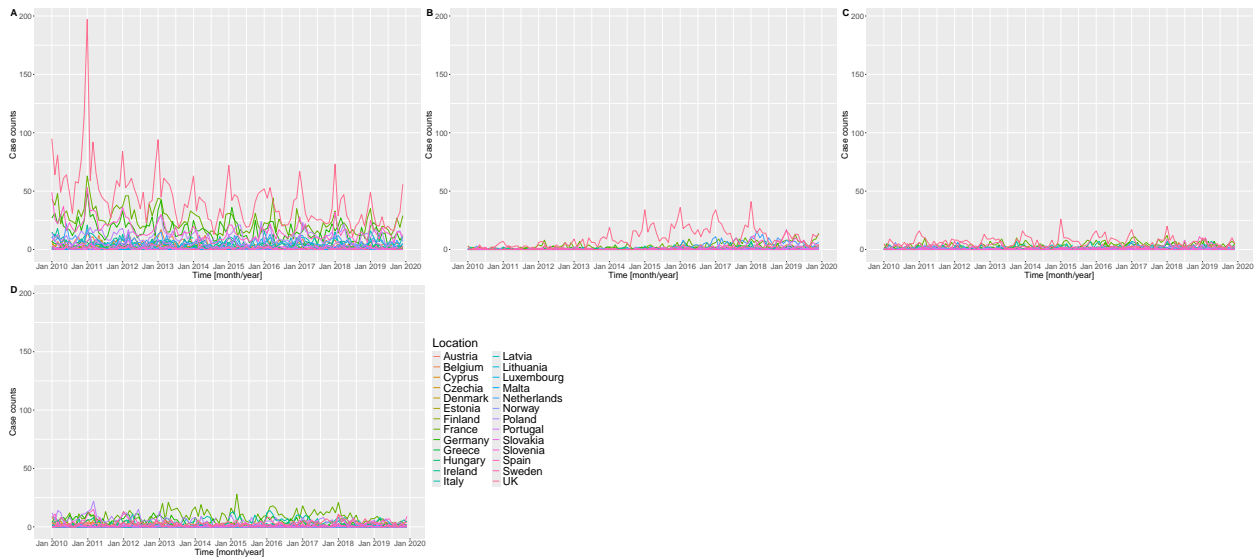


Figure S2: Monthly reported case counts of multi-type invasive meningococcal disease in 26 European countries from January 2010 to December 2019. The disease types are (A) NEIMENI-B, (B) NEIMENI-W, (C) NEIMENI-Y, and (D) NEIMENI-C.

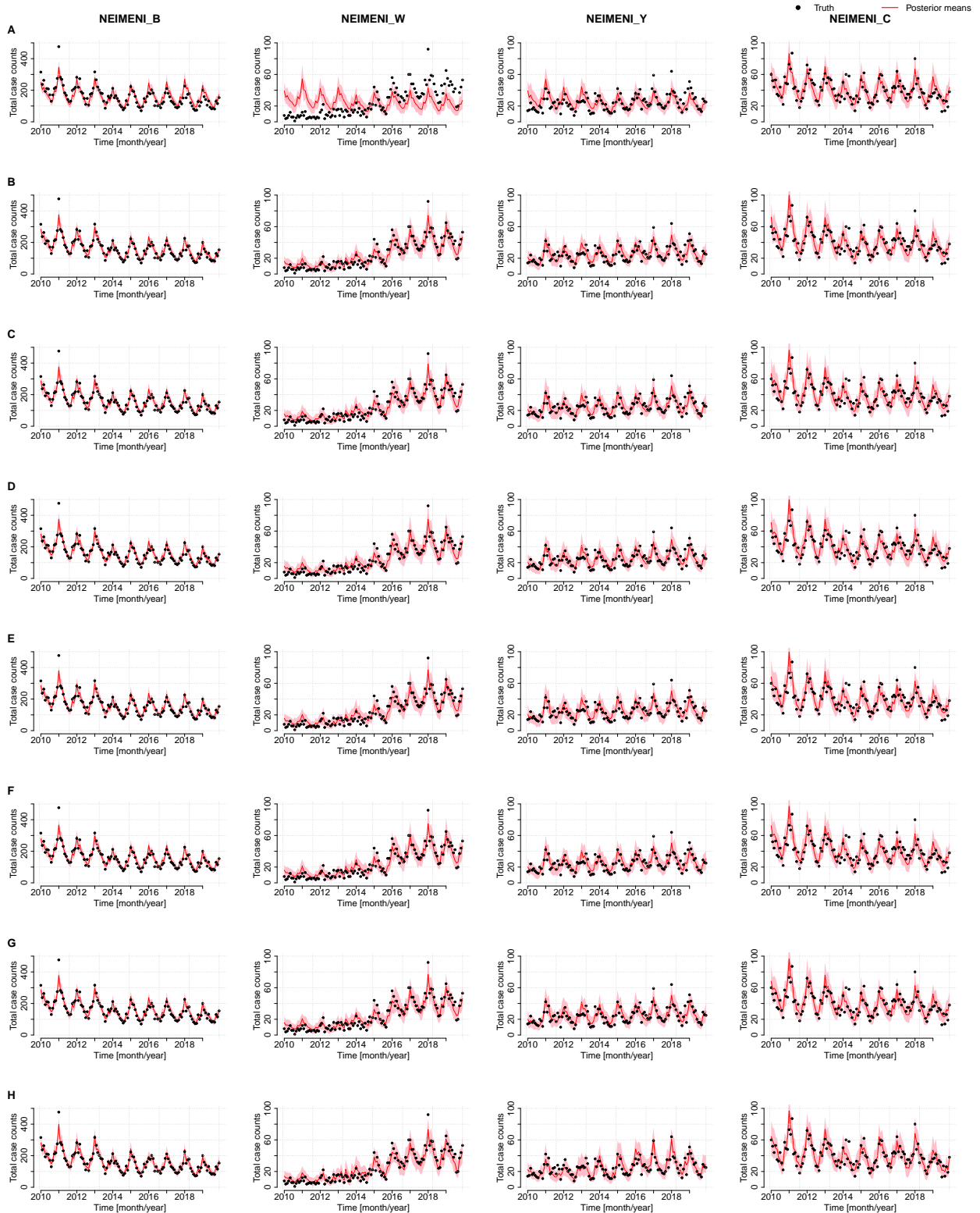


Figure S3: Posterior predictive fits for the multitype meningococcal disease analysis for the overall case counts in each serogroup across all spatial locations for (A) No epidemic model (B) Independent 1 model (C) Independent 2 model (D) Frank copula 1 model (E) Frank copula 2 model (F) Gaussian factor copula 1 model (G) Gaussian factor copula 2 model, and (H) General-dependent model. Real data shown with black dots.